

THE CENTURY OF SPACE SCIENCE

Pulsars and Isolated Neutron Stars

by

Werner Becker¹ & George Pavlov²

¹Max-Planck Institut für extraterr. Physik, Giessenbachstrasse 1,
D-85740 Garching, Germany

²Pennsylvania State University, 525 Davey Lab, University Park,
PA 16802, USA

Editors: Johan Bleeker, Johannes Geiss and Martin Huber. To be published by Kluwer Academic Publishers in "The Century of Space Science"

Original: January 2001

Revision: December 2001

Contents

8	The Milky Way – Pulsars and Isolated Neutron Stars	1
8.1	Introduction: Historical Overview	1
8.2	Physics and Astrophysics of Isolated Neutron Stars	7
8.2.1	Rotation-powered Pulsars: The Magnetic Braking Model	7
8.2.2	High-energy Emission Models	9
8.3	The Current Picture of High-Energy Emission Properties of Isolated Neutron Stars	15
8.3.1	Young Neutron Stars in Supernova Remnants	15
8.3.2	Thermal Emission from Middle-Aged Pulsars	25
8.3.3	Old Nearby Radio Pulsars	28
8.3.4	Isolated Radio-quiet Neutron Stars	30
8.3.5	Recycled Millisecond Pulsars	32
8.4	Impressive Achievements and Great Expectations	36
8.5	References	39

Chapter 8

The Milky Way – Pulsars and Isolated Neutron Stars

8.1 Introduction: Historical Overview

The idea of *neutron stars* can be traced back to early 1930's, when Subrahmanyan Chandrasekhar, whilst investigating the physics of stellar evolution, discovered that there is no way for a collapsed stellar core with a mass more than 1.4 times the solar mass, M_{\odot} , to hold itself up against gravity once its nuclear fuel is exhausted (Chandrasekhar 1931). This implies that a star left with $M > 1.4 M_{\odot}$ (the *Chandrasekhar limit*) would keep collapsing and eventually disappear from view.

After the discovery of the neutron by James Chadwick in 1932, Lev Landau was the first who speculated on the possible existence of a *star composed entirely of neutrons* (Landau 1932; Rosenfeld 1974). Using the newly-established Fermi-Dirac statistics and basic quantum mechanics, he was able to estimate that such a star, consisting of $\sim 10^{57}$ neutrons, would form a giant nucleus with a radius of the order of $R \sim (\hbar/m_n c)(\hbar c/Gm_n^2)^{1/2} \sim 3 \times 10^5$ cm, in which \hbar , c , G and m_n are the Planck constant, the speed of light, the gravitation constant and the mass of the neutron. In view of the peculiar stellar parameters, Landau called these objects “unheimliche Sterne” (weird stars), expecting that they would never be observed because of their small size and expected low optical luminosity.

Walter Baade and Fritz Zwicky were the first who proposed the idea that neutron stars could be formed in *supernovae* (Baade & Zwicky 1934). First models for the structure of neutron stars were worked out in 1939 by Robert Oppenheimer and George Volkoff, who calculated an upper limit for the neutron star mass. Using general relativistic equilibrium equations and assuming that the star is entirely described by an ideal (i.e. non-interacting) Fermi gas of neutrons, they found that any star more massive than $3 M_{\odot}$ (Oppenheimer-Volkoff limit) will suffer runaway gravitational collapse to form a black hole (Oppenheimer & Volkoff 1939). Unfortunately, their pioneering work did not predict anything astronomers could actually observe, and the idea of neutron stars was not taken seriously by the astronomical community. Neutron stars therefore had remained in the realm of imagination for nearly a quarter of century, until in the 60's a series of epochal discoveries were made in high-energy and radio astronomy.

X-rays and gamma-rays can only be observed from above the earth's atmosphere¹, which requires detectors to operate from high flying balloons, rockets or satellites. One of the first X-ray detectors brought to space was launched by Herbert Friedman and his team at the Naval Research Laboratory in order to investigate the influence of solar activity on the propagation of radio signals in the earth's atmosphere (cf. H. Friedman, this book). Using simple proportional counters put on old V-2 (captured in Germany after the World War II) and Aerobee rockets, they were the first who detected X-rays from the very hot gas in the solar corona. However, the intensity of this radiation was found to be a factor 10^6 lower than that measured at optical wavelengths. In the late

¹X-rays are absorbed at altitudes 20–100 km.

50's, it was therefore widely believed that all other stars, much more distant than the Sun, should be so faint in X-rays that further observations at that energy range would be hopeless. On the other hand, results from high-energy cosmic ray experiments suggested that there exist celestial objects (e.g. supernova remnants) which produce high-energy cosmic rays in processes which, in turn, may also produce X-rays and gamma-rays (Morrison et al. 1954, Morrison 1958). These predictions were confirmed in 1962, when the team led by Bruno Rossi and Riccardo Giacconi accidentally detected X-rays from Sco X-1. With the aim to search for fluorescent X-ray photons from the Moon², they launched an Aerobee rocket on 12 June 1962 from White Sands (New Mexico) with three Geiger counters as payload, each having a $\sim 100^\circ$ field of view and an effective collecting area of about 10 cm^2 (Giacconi 1974). The experiment detected X-rays not from the Moon but from a source located in the constellation Scorpio, dubbed as Sco X-1, which is now known as the brightest extra-solar X-ray source in the sky. Evidence for a weaker source in the Cygnus region and the first evidence for the existence of a diffuse isotropic X-ray background was also reported from that experiment (Giacconi et al. 1962). Subsequent flights launched to confirm these first results detected Tau X-1, a source in the constellation Taurus which coincided with the Crab supernova remnant (Bowyer et al. 1964). Among the various processes proposed for the generation of the detected X-rays was *thermal radiation from the surface of a hot neutron star* (Chiu & Salpeter 1964), and searching for this radiation has become a strong motivation for further development of X-ray astronomy. However, the X-ray emission from the Crab supernova remnant was found to be of a finite angular size (~ 1 arcmin) whereas a neutron star was expected to appear as a point source. Thus, the early X-ray observations were not sensitive enough to prove the existence of neutron stars. This was done a few years later by radio astronomers.

In 1967, Jocelyn Bell, a graduate student under the supervision of Anthony Hewish at the Cambridge University of England, came across a series of pulsating radio signals while using a radio telescope specially constructed to look for rapid variations in the radio emission of quasars. These radio pulses, 1.32 seconds apart, with remarkable clock-like regularity, were emitted from an unknown source in the sky at right ascension $19^{\text{h}} 20^{\text{m}}$ and declination $+23^\circ$. Further observations refined the pulsating period to 1.33730113 seconds. The extreme precision of the period suggested at first that these signals might be generated by extraterrestrial intelligence. They were subsequently dubbed as LGM1, an acronym for “Little Green Man 1” (Bell 1977). However, as a few more similar sources had been detected, it became clear that a new kind of celestial objects was discovered. The link between these pulsating radio sources, which were called *pulsars*, and fast spinning neutron stars was provided by Franco Pacini (1967, 1968) and Thomas Gold (1968, 1969). Pacini, then a young postdoc at the Cornell University, had published a paper a few months before the discovery by Bell and Hewish in which he proposed that the *rapid rotation of a highly magnetized neutron star* could be the source of energy in the Crab Nebula. This prediction was based on the pioneering work of Hoyle, Narlikar and Wheeler (1964), who had proposed that a magnetic field of 10^{10} Gauss might exist on a neutron star at the center of the Crab Nebula. The most fundamental ideas on the nature of the pulsating radio sources were published by Gold (1968; 1969) in two seminal *Nature* papers. In these papers Gold introduced the concept of the *rotation-powered pulsar* which radiates at the expense of its rotational energy (pulsar spins down as rotational energy is radiated away) and recognized that the rotational energy is lost via electromagnetic radiation of the rotating magnetic dipole and emission of relativistic particles. The particles are accelerated in the pulsar magnetosphere along the curved magnetic field lines and emit the observed intense curvature and synchrotron radiation³.

Since those early days of pulsar astronomy more than 1000 radio pulsars have been discovered (see, e.g., the catalog by Taylor, Manchester & Lyne 1993 which lists about half of them). The

²The Moon was selected as a target because it was expected that a state-of-the-art detector available at that time would not be sensitive enough to detect X-rays from extra-solar sources. “We felt [...] that it would be very desirable to consider some intermediate target which could yield concrete results while providing a focus for the development of more advanced instrumentation which ultimately would allow us to detect cosmic X-ray sources” (Giacconi 1974).

³When a charged relativistic particle moves along a curved magnetic field line, it is accelerated transversely and radiates. This *curvature radiation* is closely related to *synchrotron radiation* caused by gyration of particles around the magnetic field lines.

discovery of the first radio pulsar was very soon followed by the discovery of two most famous pulsars, the fast 33 ms pulsar in the Crab Nebula (Staelin & Reifenstein 1968) and the 89 ms pulsar in the Vela supernova remnant (Large et al. 1968). The fact that these pulsars are located within supernova remnants provided striking confirmation that neutron stars are born in core collapse supernovae from massive main sequence stars. These exciting radio discoveries triggered subsequent pulsar searches at nearly all wavelengths.

Cocke, Disney & Taylor (1969) discovered optical pulses from the Crab pulsar, whereas its X-ray pulsations in the 1.5–10 keV range were discovered by Friedman’s group at the Naval Research Laboratory (Fritz et al. 1969) and by the team of the Massachusetts Institute of Technology (Bradt et al. 1969) three months later. Using a plastic scintillator platform, Hillier et al. (1970) flew a balloon-borne experiment over southern England and detected its pulsed gamma-rays at a $\sim 3.5\sigma$ level at energies greater than 0.6 MeV. These early multi-wavelength observations showed that the pulses are all phase-aligned, with a pulse profile which was very nearly the same at all wavelengths, suggesting a common emission site for the radiation. Moreover, the power observed at the high photon energies exceeded that in the optical band by more than two orders of magnitude, justifying the need for more sensitive satellite-based X-ray and gamma-ray observatories to perform more detailed investigations of the emission mechanism of pulsars and to survey the sky for other X-ray and gamma-ray sources.

The first earth-orbiting mission dedicated entirely to celestial X-ray astronomy, *SAS-1* (Small Astronomy Satellite 1), was launched by NASA in December 1970 from a launch site in Kenya. The observatory, later named *Uhuru*⁴, was sensitive in the range 2 – 20 keV and equipped with two sets of proportional counters having a collecting area of 840 cm² (Giacconi et al. 1971). It was designed to operate in survey mode, allowing for the first time to scan the whole sky with a sensitivity of 1.5×10^{-11} ergs s⁻¹cm⁻². In somewhat more than two years of very successful operation, 339 new X-ray sources were detected (Forman et al. 1978), belonging to the group of accreting binaries, supernova remnants, Seyfert galaxies and clusters of galaxies. By far the largest sample of objects was found to belong to the group of accretion-powered pulsars — neutron stars in binary systems accreting matter from a companion star. As the matter spirals in onto the neutron star surface or heats up in an accretion disc, strong X-ray radiation is emitted (van den Heuvel et al., this book).

The next major step in high-energy astronomy was the launch of *SAS-2* in November 1972, the first satellite dedicated exclusively to gamma-ray astronomy (Fichtel et al. 1975). The detector, a spark chamber, was sensitive in the energy range 35–1000 MeV. Although the mission lasted only seven months and ended by a failure of the low-voltage power supply, its measurements confirmed the existence of the gamma-ray pulses from the Crab (Kniffen et al. 1974) and discovered the gamma-ray pulses from the Vela pulsar (Thompson et al. 1975), which was found to be the strongest gamma-ray source in the sky. The Vela lightcurve was characterized by two relatively sharp peaks, separated by 0.4 in phase (as observed for the Crab) but not phase-aligned with the radio and optical pulses.

In addition, a few unidentified gamma-ray sources were detected, among them *Geminga*⁵, a faint source in the Gemini region from which ~ 100 γ -ray photons had been recorded, but which had to await its final identification about 20 years later. Gamma-ray astronomy, from its beginning, was often hampered by the relatively small number of detected photons and large position error boxes, typically $\sim 0.5^\circ - 1^\circ$. This position uncertainty strongly complicated follow-up observations for optical and X-ray counterparts. Scientific publications describing data analysis techniques optimized for ‘sparse data’, particularly the timing analysis aimed at pulsation search, were therefore always ranked high on the gamma-ray market.

The first complete and detailed gamma-ray map of the Galaxy was provided by the ESA mission *COS-B*, launched in August 1975. Developed under the responsibility of a group of

⁴Uhuru means ‘freedom’ in Swahili.

⁵The source was dubbed with the name Geminga, a pun in Milanese dialect in which *gh’è minga* means *it is not there or it does not exist*, by Giovanni Bignami — see Bignami & Caraveo (1996) for a comprehensive description of the Geminga story, from the first discovery to the final identification. It is amusing to note, the name *Geminga* inspired Eric Cohez to choose the title of his science fiction book *Geminga: la civilization perdue*.

European research laboratories known as the Caravane Collaboration⁶, the satellite carried two scientific payloads, a digital spark chamber, sensitive in the range 0.03 – 5 GeV, and a 2 – 12 keV collimated proportional counter which was used as a pulsar synchronizer. Because of a not very accurate on-board clock calibration, the latter was to ensure the synchronization of the X-ray and gamma-ray pulses from isolated pulsars, like the Crab and Vela pulsars, and accreting pulsars in X-ray binaries. It was further used to determine pulsar ephemeris from the temporal analysis of X-ray data, independently from the availability of exact radio ephemeris. The high sensitivity of the gamma-ray detector allowed Kanbach et al. (1980) to conduct the first detailed temporal and spectral study of the Vela pulsar in the range 0.05 – 3 GeV. The pulsar’s spectrum was found to be represented by a power-law $dN/dE \propto E^{-\alpha}$ (with a photon index of $\alpha = 1.89 \pm 0.06$ for the phase-averaged spectrum), but appreciable differences of the photon index were detected for different pulsar phases (e.g., the inter-pulse emission, first detected in the *COS-B* data, was found to have the hardest spectrum). The *COS-B* observations of the Crab pulsar provided much improved photon statistics which resulted in a more accurate pulse profile (Wills et al. 1982) and detailed spectral studies (Clear et al. 1987).

Many radio pulsars had been observed by mid-seventies, and two of them, the Crab and Vela pulsars, had been detected at high photon energies. Although the interpretation of both isolated and accreting pulsars as neutron stars with enormous magnetic fields, $\sim 10^{12}$ G, had been generally accepted, no direct evidence on the existence of such huge fields had been obtained. This evidence came from a remarkable spectral observation of Hercules X-1, an accreting binary pulsar discovered with *Uhuru* by Tananbaum et al. (1972). On May 3, 1976, a team of the Max-Planck Institut für extraterrestrische Physik in Garching and the Astronomische Institut of the University of Tübingen, led by Joachim Trümper, launched from Palestine (Texas) a balloon experiment, equipped with a collimated NaI scintillation counter and a NaI-CsI-phoswich detector, sensitive in the range 15 – 160 keV. They easily detected the 1.24 s pulsations up to 80 keV (Kendziorra et al. 1977). However, when Bruno Sacco and Wolfgang Pietsch attempted to fit the observed spectrum with usual continuum spectral models, they found that a one-component continuum model cannot represent the data — all fits gave unacceptably large residuals at $\sim 40 - 60$ keV. Further data analysis confirmed that the spectral feature was not an artifact (e.g., due to incomplete shielding of the in-flight calibration source ²⁴¹Am, which emitted a spectral line at E=59.5 keV). It was Joachim Trümper who first recognized that the excess emission at 58 keV (or an absorption feature at 42 keV, depending on interpretation – cf. Fig.8.1) could be associated with the resonant electron cyclotron emission or absorption in the hot polar plasma of the rotating neutron star. The corresponding magnetic field strength would then be 6×10^{12} or 4×10^{12} G (Trümper et al. 1978). This observation provided the first direct measurement of a neutron star magnetic field and confirmed the basic theoretical predictions that neutron stars are highly magnetized, fast spinning compact objects.

Beginning in 1977, NASA launched a series of large scientific payloads called *High Energy Astrophysical Observatories*⁷: HEAO 1 (Aug 1977–Jan 1979), HEAO 2 (Nov 1978–Apr 1981), and HEAO 3 (Sep 1979–May 1981). Particularly important results on isolated neutron stars, among many other X-ray sources, were obtained with *HEAO 2*, widely known as the *Einstein* X-ray observatory (Giacconi et al. 1979), which carried the first imaging X-ray telescope on a satellite. Among four focal plane detectors of *Einstein*, two proved to be particularly useful for detecting and studying isolated neutron stars. The High Resolution Imager (HRI), a micro-channel plate detector, sensitive in the 0.15 – 4 keV energy band, with about 5 arcsec angular resolution, was designed to use the imaging capability of the X-ray telescope. However, it had no energy resolution and its field of view was small, $\simeq 25$ arcmin. The Imaging Proportional Counter (IPC), the workhorse of the observatory, could detect weaker sources than the HRI and had a wider field of view, $\simeq 1^\circ$, but its imaging resolution was about 1 arcmin. It was capable of studying spectra with modest energy resolution in the range 0.2 – 4 keV.

⁶formed of members from MPE-Garching, CEN-Saclay, SRON-Leiden (today Utrecht), IFCAI-Palermo, CNR-Milano and SSD-ESTEC.

⁷The dramatic history of the HEAO project and the experiments on board of HEAO satellites are lively described by Wallace Tucker (1984).

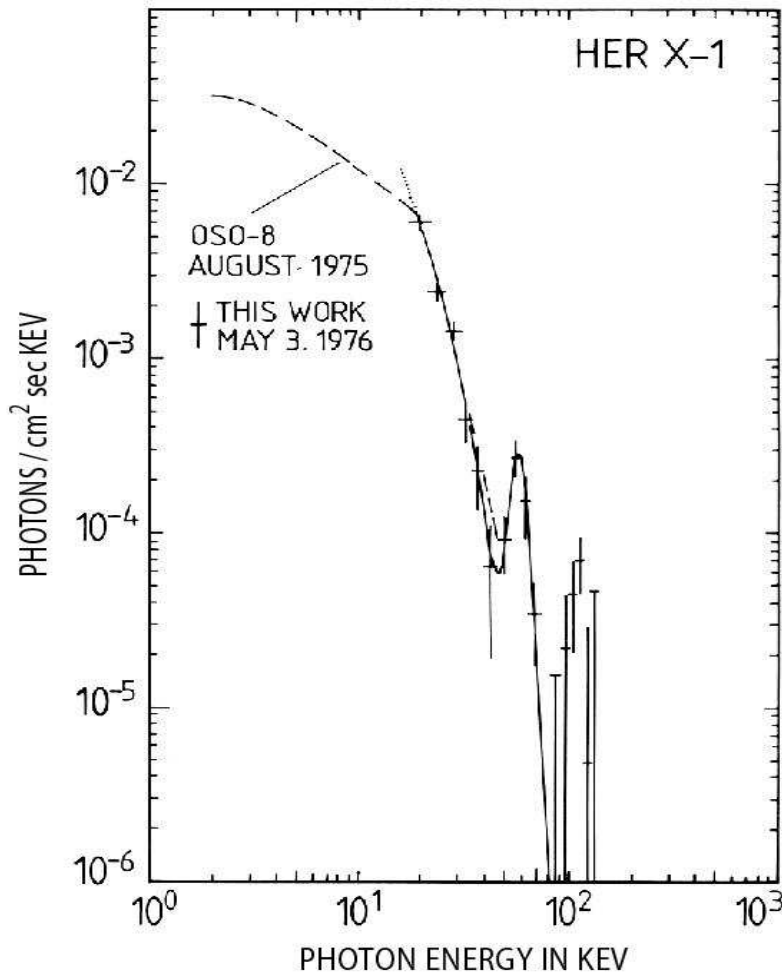


Figure 8.1: Unfolded X-ray spectrum from Hercules X-1 (from Trümper et al. 1978), showing the first measurement of a cyclotron line in a pulsed spectrum of an accreting neutron star.

Einstein investigated the soft X-ray radiation from the previously known Crab and Vela pulsars and resolved the compact nebula around the Crab pulsar (Harnden & Seward 1984). It discovered pulsed X-ray emission from two other very young pulsars, PSR B0540–69 in the Large Magellanic Cloud (Seward, Harnden, & Helfand 1984) and PSR B1509–58 (Seward & Harnden 1982), with periods 50 ms and 150 ms, respectively. Interestingly, these pulsars were the first ones discovered in the X-ray band and only subsequently at radio frequencies. No pulsations from the Vela pulsar were found in the soft X-ray band.

Einstein also detected three middle-aged radio pulsars, PSR B0656+14 (Córdova et al. 1989), B1055–52 (Cheng & Helfand 1983), and B1951+32 (Wang & Seward 1984). Also, X-ray counterparts of two nearby old radio pulsars, PSR B0950+08 and B1929+10, were identified, based on positional coincidence (Seward & Wang 1988). In addition, many supernova remnants were mapped — 47 in our Galaxy (Seward 1990) and 10 in the Magellanic Clouds (Long & Helfand 1979), and several neutron star candidates were detected as faint, soft point sources close to the centers of the supernova remnants RCW 103 (Tuohy & Garmire 1980), PKS 1209–51/52 (Helfand & Becker 1984), Puppis A (Petre et al. 1982) and Kes 73 (Kriss et al. 1985).

Some additional information on isolated neutron stars was obtained by *EXOSAT* (*European X-ray Observatory Satellite* — see Taylor et al. 1981), which was equipped with a low-energy detector with imaging capability and grating (0.04–2 keV) and a medium-energy proportional counter (1.5–50 keV). In particular, it measured the soft X-ray spectra of the middle-aged pulsar

PSR B1055–52 (Brinkmann & Ögelman 1987) and of a few neutron star candidates in supernova remnants (e.g., PKS 1209–51/52 – Kellett et al. 1987).

In spite of the major advance in the field of high-energy astronomy provided by the space observatories (particularly, by *Einstein*) in the 70’s–80’s, the results on isolated neutron stars made it clear that more sensitive instruments and multi-wavelength observations were required to understand the spatial, temporal and spectral emission properties of these objects. For instance, *Einstein* was able to detect X-ray pulses only from the young and powerful Crab-like pulsars, whereas only flux estimates could be obtained for the other detected neutron stars. Only two pulsars, Crab and Vela, were detected in the gamma-ray and optical ranges.

The situation improved drastically in the last decade of the century, which can be seen as the “decade of space science”. The first X-ray satellite in a series of several launched to explore the Universe from space was the German/US/UK mission *ROSAT* (*Röntgen Satellit* – see Trümper 1983), sensitive in the 0.1 – 2.4 keV band. Equipped with an imaging X-ray telescope and three detectors, Position Sensitive Proportional Counter (PSPC), High Resolution Imager (HRI) and EUV Wide-Field Camera, the observatory performed very successful observations of all kinds of astronomical objects in more than eight years of its life (June 1990 – Feb. 1999). During the first 6 months of the mission, the *ROSAT All-Sky Survey*, with the limiting sensitivity of $\sim 3 \times 10^{-12} \text{ erg s}^{-1} \text{ cm}^{-2}$, provided valuable information on fluxes for all the known radio pulsars. This, in particular, made it possible to constrain the neutron star cooling scenarios on a large sample of these objects (Becker, Trümper & Ögelman 1993; Becker 1995).

The complement to *ROSAT*, covering the harder X-ray band 1 – 10 keV, was the Japanese/US mission *ASCA* (*Advanced Satellite for Cosmology and Astrophysics* – see Tanaka et al. 1994), launched in 1993. It was the first X-ray observatory equipped with a charge-coupled-device (CCD) imager – the Solid-state Imaging Spectrometer (SIS), with a much better spectral resolution than the *ROSAT* PSPC. The Gas Imaging Spectrometer (GIS), which was operated in parallel, provided timing information in addition. Launched in 1992, the *EUVE* (*Extreme Ultraviolet Explorer* – see Bowyer 1990), sensitive in the range 70 – 760 Å, has been able to observe several neutron stars at very soft X-rays, 0.07 – 0.2 keV. The contributions to the neutron star research, provided by the instruments aboard the Italian/Dutch X-ray mission *BeppoSAX* (Butler & Scarsi 1990), sensitive in the range of 0.1 – 200 keV, and the USA’s *RXTE* (*Rossi X-ray Timing Explorer* – see Bradt, Swank & Rothschild 1990), both launched in the mid-90’s, were particularly useful for studying X-ray binaries, including accretion-powered pulsars (see van den Heuvel et al., this book).

The new advance in the study of gamma-ray emission from neutron stars was provided by nine years (1991 – 2000) of operation of *CGRO* (*Compton Gamma-Ray Observatory* – see Kniffen 1990), which has explored the gamma-ray sky in the broad range from 50 keV to 30 GeV with four instruments. Particularly useful for observations of isolated neutron stars was the Energetic Gamma-Ray Experiment Telescope (EGRET), which detected five new gamma-ray pulsars (Thompson et al. 1999), in addition to the previously observed Crab and Vela pulsars. In particular, the gamma-ray source Geminga, known since 1972, was identified as a pulsar (Bertsch et al. 1992) after the discovery of coherent pulsations in X-rays with *ROSAT* (Halpern & Holt 1992).

Finally, the outstanding capabilities of the *Hubble Space Telescope* (*HST*), launched in 1990, enabled astronomers to directly observe neutron stars, despite their extremely small size, in the IR/optical/UV range (see Fig.8.12), which appeared completely impossible a few decades ago. Of particular interest was the discovery of the (presumably thermal) optical-UV radiation from old neutron stars (Pavlov, Stringfellow & Córdoba 1996a; Walter & Matthews 1997).

Our current understanding of the high-energy emission of neutron stars, summarized in Section 8.3, is largely based on the results obtained with these space observatories. Although some of them have completed their service and rest on the ocean bottom, new and more powerful X-ray missions have taken their place just before the onset of the new century — *Chandra*, with the outstanding imaging capability of its telescope and *XMM-Newton* with its unprecedentedly high spectral sensitivity and collecting power. It is therefore safe to say that in the very near future a wealth of new X-ray data on various astronomical objects, including isolated neutron stars, will become available and will have a major impact on our current understanding of these objects.

8.2 Physics and Astrophysics of Isolated Neutron Stars

Neutron stars represent unique astrophysical laboratories which allow us to explore the properties of matter under the most extreme conditions observable in nature⁸. Studying neutron stars is therefore an interdisciplinary field, where astronomers and astrophysicist work together with a broad community of physicists. Particle, nuclear and solid-state physicists are strongly interested in the internal structure of neutron stars which is determined by the behavior of matter at densities above the nuclear density $\rho_{\text{nuc}} = 2.8 \times 10^{14} \text{ g cm}^{-3}$. Plasma physicists are modeling the pulsar emission mechanisms using electrodynamics and general relativity. It is beyond the scope of this section to describe in detail the current status of the theory of neutron star structure or the magnetospheric emission models. We rather refer the reader to the literature (Michel 1991; Beskin, Gurevich & Istomin 1993; Glendenning 1996; Weber 1999) and provide only the basic theoretical background relevant to section 8.3 which summarizes the observed high-energy emission properties of rotation-powered pulsars and radio-quiet neutron stars.

8.2.1 Rotation-powered Pulsars: The Magnetic Braking Model

Following the ideas of Pacini (1967, 1968) and Gold (1968, 1969), the more than 1000 radio pulsars detected so far can be interpreted as rapidly spinning, strongly magnetized neutron stars radiating at the expense of their rotational energy. This very useful concept allows one to obtain a wealth of information on basic neutron star/pulsar parameters just from measuring the pulsar's period and period derivative. Using the Crab pulsar as an example will make this more clear. A neutron star with a canonical radius of $R = 10 \text{ km}$ and a mass of $M = 1.4 M_{\odot}$ has a moment of inertia $I \approx (2/5)MR^2 \approx 10^{45} \text{ g cm}^2$. The Crab pulsar spins with a period of $P = 33.403 \text{ ms}$. The rotational energy of such a star is $E_{\text{rot}} = 2\pi^2 I P^{-2} \approx 2 \times 10^{49} \text{ erg}$. This is comparable with the energy released in thermonuclear burning by a usual star over many million years. Very soon after the discovery of the first radio pulsars it was noticed that their spin periods increase with time. For the Crab pulsar, the period derivative is $\dot{P} = 4.2 \times 10^{-13} \text{ s s}^{-1}$, implying a decrease in the star's rotation energy of $dE_{\text{rot}}/dt \equiv \dot{E}_{\text{rot}} = -4\pi^2 I \dot{P} P^{-3} \approx 4.5 \times 10^{38} \text{ erg s}^{-1}$. Ostriker & Gunn (1969) suggested that the pulsar slow-down is due to the braking torque exerted on the neutron star by its magneto-dipole radiation, that yields $\dot{E}_{\text{brak}} = -(32\pi^4/3c^3) B_{\perp}^2 R^6 P^{-4}$ for the energy loss of a rotating magnetic dipole, where B_{\perp} is the component of the equatorial magnetic field perpendicular to the rotation axis. Equating \dot{E}_{brak} with \dot{E}_{rot} , we find $B_{\perp} = 3.2 \times 10^{19} (P \dot{P})^{1/2}$ Gauss. For the Crab pulsar, this yields $B_{\perp} = 3.8 \times 10^{12} \text{ G}$. From $\dot{E}_{\text{rot}} = \dot{E}_{\text{brak}}$ one further finds that $\dot{P} \propto P^{-1}$, for a given B_{\perp} . This relation can be generalized as $\dot{P} = k P^{2-n}$, where k is a constant, and n is the so-called braking index ($n = 3$ for the magneto-dipole braking). Assuming that the initial rotation period P_0 at the time t_0 of the neutron star formation was much smaller than today, at $t = t_0 + \tau$, we obtain $\tau = P/[(n-1)\dot{P}]$, or $\tau = P/(2\dot{P})$ for $n = 3$. This quantity is called the characteristic spin-down age. It is a measure for the time span required to lose the rotational energy $E_{\text{rot}}(t_0) - E_{\text{rot}}(t)$ via magneto-dipole radiation. For the Crab pulsar one finds $\tau = 1258 \text{ yrs}$. As the neutron star in the Crab supernova remnant is the only pulsar for which its historical age is known (the Crab supernova was observed by Chinese astronomers in 1054 AD), we see that the spin-down age exceeds the true age by about 25%. Although the spin-down age is just an estimate for the true age of the pulsar, it is the only one available for pulsars other than the Crab, and it is commonly used in evolutionary studies (e.g., neutron star cooling).

A plot of observed periods versus period derivatives is shown in Figure 8.2, using the pulsars from the Princeton Pulsar Catalog (Taylor et al. 1993). Such a P - \dot{P} diagram is extremely useful for classification purposes. The colored symbols represent those 35 pulsars which, by the end of 2000, have been detected at X-ray energies. Among them are the 7 gamma-ray pulsars indicated by green color. The objects in the upper right corner represent the soft-gamma-ray repeaters (SGRs) and anomalous X-ray pulsars (AXPs) which have been suggested to be magnetars (see 8.3.1.4).

⁸Although black holes are even more compact than neutron stars, they can only be observed through the interaction with their surroundings.

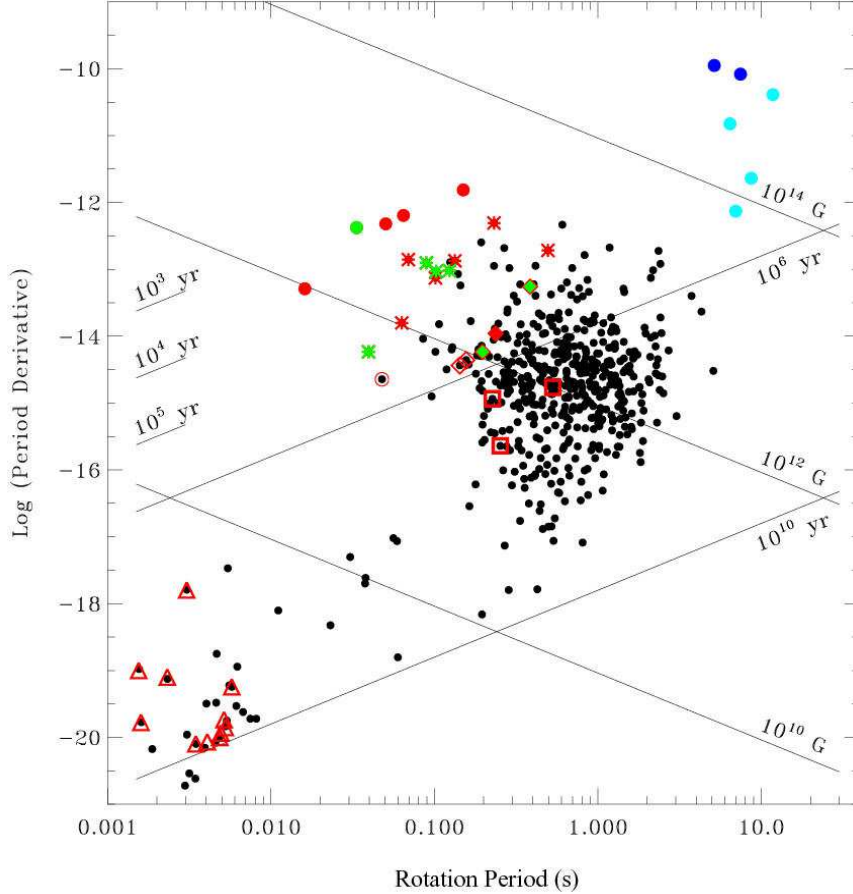


Figure 8.2: The $P - \dot{P}$ diagram — distribution of rotation-powered pulsars (small black dots) over their spin parameters. The straight lines correspond to constant ages $\tau = P/(2\dot{P})$ and magnetic field strengths $B_{\perp} = 3.2 \times 10^{19} (P\dot{P})^{1/2}$. Separate from the majority of ordinary-field pulsars are the millisecond pulsars in the lower left corner and the putative magnetars — soft gamma-ray repeaters (dark blue) and anomalous X-ray pulsars (light blue) in the upper right. Although magnetars and anomalous X-ray pulsars are not rotation-powered, they are included in this plot to visualize their estimated superstrong magnetic fields. X-ray detected pulsars are indicated by colored symbols. Green symbols indicate gamma-ray pulsars.

Although the magnetic braking model is generally accepted, the *observed* spin-modulated emission, which gave pulsars their name, is found to account only for a small fraction of \dot{E} . The efficiencies, $\eta = L/\dot{E}$, observed in the radio and optical bands are typically in the range $\sim 10^{-7} - 10^{-5}$, whereas they are about $10^{-4} - 10^{-3}$ and $\sim 10^{-2} - 10^{-1}$ at X-ray and gamma-ray energies, respectively. It has therefore been a long-standing question how rotation-powered pulsars lose the bulk of their rotational energy.

The fact that the energy loss of rotation-powered pulsars cannot be fully accounted for by the magneto-dipole radiation is known from the investigation of the pulsar braking index, $n = 2 - P\ddot{P}\dot{P}^{-2}$. Pure dipole radiation would imply a braking index $n = 3$, whereas the values observed so far are $n = 2.515 \pm 0.005$ for the Crab (Lyne et al. 1988), $n = 2.8 \pm 0.2$ for PSR B1509–58 (Kaspi et al. 1994), $n = 2.28 \pm 0.02$ for PSR B0540–69 (Boyd et al. 1995), and $n = 1.4 \pm 0.2$ for the Vela pulsar (Lyne et al. 1996). The deviation from $n = 3$ is usually taken as evidence that a significant fraction of the pulsar’s rotational energy is carried off by a pulsar wind, i.e., a mixture of charged particles and electromagnetic fields, which, if the conditions are appropriate, forms a *pulsar-wind nebula* observable at optical, radio and X-ray energies. Such pulsar-wind nebulae (often called plerions or synchrotron nebulae) are known so far *only* for few young and

powerful (high \dot{E}) pulsars and for some center-filled supernova remnants, in which a young neutron star is expected, but only emission from its plerion is detected. The mechanisms of pulsar wind generation and its interaction with the ambient medium are poorly understood.

Thus, the popular model of magnetic braking provides plausible estimates for the neutron star magnetic field B_{\perp} , its rotational energy loss \dot{E} , and characteristic age τ , but it does not provide any detailed information about the physical processes which operate in the pulsar magnetosphere and which are responsible for the broad-band spectrum, from the radio to the X-ray and gamma-ray bands (see Fig.8.16). As a consequence, there exist a number of magnetospheric emission models, but no generally accepted theory.

8.2.2 High-energy Emission Models

Although rotation-powered pulsars are most widely known for their radio emission, the mechanism of the radio emission is poorly understood. However, it is certainly different from those responsible for the high-energy (infrared through gamma-ray) radiation observed with space observatories. It is well known that the radio emission of pulsars is a coherent process, and the coherent curvature radiation has been proposed as the most promising mechanism (see Michel 1991, and references therein). On the other hand, the optical, X-ray and gamma-ray emission observed in pulsars must be incoherent. Therefore, the fluxes in these energy bands are directly proportional to the densities of the radiating high-energy electrons in the acceleration regions, no matter which radiation process (synchrotron radiation, curvature radiation or inverse Compton scattering) is at work at a given energy. High-energy observations thus provide the key for the understanding of the pulsar emission mechanisms. So far, the high-energy radiation detected from rotation-driven pulsars has been attributed to various thermal and non-thermal emission processes including the following:

- Non-thermal emission from charged relativistic particles accelerated in the pulsar magnetosphere. As the energy distribution of these particles follows a power-law, the emission is also characterized by power-law-like spectra in broad energy bands. The emitted radiation can be observed from optical to the gamma-ray band.
- Extended emission from pulsar-driven synchrotron nebulae. Depending on the local conditions (density of the ambient interstellar medium), these nebulae can be observed from radio through hard X-ray energies.
- X-ray and gamma-ray emission from interaction of relativistic pulsar winds with a close companion star or with the wind of a companion star, in binary systems (see Arons & Tavani 1993).
- Photospheric emission from the hot surface of a cooling neutron star. In this case a modified black-body spectrum and smooth, low-amplitude intensity variations with the rotational period are expected, observable from the optical through the soft X-ray range (cf. Greenstein & Hartke 1983; Romani 1987; Pavlov et al. 1995).
- Thermal soft X-ray emission from the neutron star's polar caps which are heated by the bombardment of relativistic particles streaming back to the surface from the pulsar magnetosphere (Kundt & Schaaf 1993; Pavlov et al. 1994).

In the following subsections we will briefly present the basic ideas on the magnetospheric emission models as well as material relevant to neutron star cooling and thermal emission from the neutron star surface.

8.2.2.1 Magnetospheric Emission Models

So far, there is no consensus as to where the pulsar high-energy radiation comes from (see for example Michel 1991; Beskin et al. 1993 and discussion therein). There exist two main types of

models — the *polar cap models*, which place the emission zone in the immediate vicinity of the neutron star’s polar caps, and the *outer gap models*, in which this zone is assumed to be close to the pulsar’s light cylinder⁹ to prevent materializing of the photons by the one-photon pair creation in the strong magnetic field, according to $\gamma + B \rightarrow e^+ + e^-$ (see Fig.8.3). The gamma-ray emission in the polar cap models (Arons & Scharlemann 1979; Daugherty & Harding 1996; Sturmer & Dermer 1994) forms a hollow cone centered on the magnetic pole, producing either double-peaked or single-peaked pulse profiles, depending on the observer’s line of sight. The outer gap model was originally proposed to explain the bright gamma-ray emission from the Crab and Vela pulsars (Cheng, Ho & Ruderman 1986a,b) as the efficiency to get high-energy photons out of the high B-field regions close to the surface is rather small. Placing the gamma-ray emission zone at the light cylinder, where the magnetic field strength is reduced to $B_L = B (R/R_L)^3$, provides higher gamma-ray emissivities which are in somewhat better agreement with the observations. In both types of models, the high-energy radiation is emitted by relativistic particles accelerated in the very strong electric field, $\mathcal{E} \sim (R/cP)B$, generated by the magnetic field co-rotating with the neutron star. These particles are generated in cascade (avalanche) processes in charge-free gaps, located either above the magnetic poles or at the light cylinder. The main photon emission mechanisms are synchrotron/curvature radiation and inverse Compton scattering of soft thermal X-ray photons emitted from the hot neutron star surface.

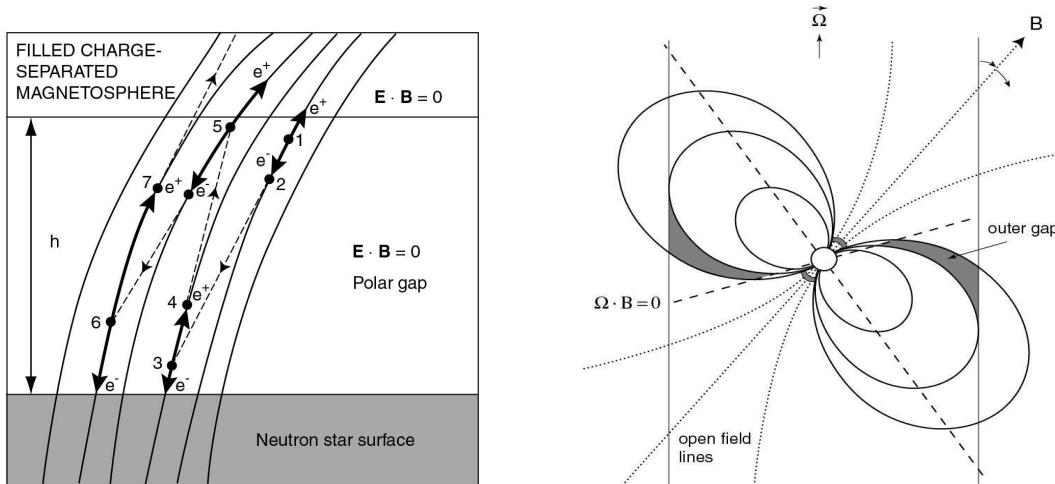


Figure 8.3: Geometry of the acceleration zones as they are defined in the polar cap model (left), according to Ruderman & Sutherland (1975), and outer gap model (right), according to Cheng, Ho & Ruderman (1986a,b). The polar cap model predicts “pencil” beams emitted by particles accelerated along the curved magnetic field lines. According to the outer gap model, the pulsar radiation is emitted in “fan” beams. Being broader, the latter can easier explain two (and more) pulse components observed in several gamma-ray pulsars.

In recent years the polar-cap and outer-gap models have been further developed (e.g., Sturmer, Dermer & Michel 1995; Harding & Muslimov 1998; Zhang & Harding 2000; Romani & Yadigaroglu 1995; Romani 1996), incorporating the new results on gamma-ray emission from pulsars obtained with the Compton Gamma-Ray Observatory. At the present stage, the observational data can be interpreted with any of the two models, albeit under quite different assumptions on pulsar parameters (e.g., on the direction of the magnetic and rotational axes). The critical observations to distinguish between the two models include measuring the relative phases between the peaks of the pulse profiles at different energies. We expect that multi-wavelength timing of a large sample of pulsars with the aid of the Chandra, XMM-Newton, Integral and the Hubble Space Observatory will resolve this problem in a few years.

⁹The light cylinder is a virtual cylinder whose radius, $R_L = cP/(2\pi)$, is defined by the condition that the azimuthal velocity of the co-rotating magnetic field lines is equal to the speed of light.

8.2.2.2 Thermal Evolution of Neutron Stars

Neutron stars are formed at very high temperatures, $\sim 10^{11}$ K, in the imploding cores of supernova explosions. Much of the initial thermal energy is radiated away from the interior of the star by various processes of neutrino emission (mainly, Urca processes and neutrino bremsstrahlung), leaving a one-day-old neutron star with an internal temperature of about $10^9 - 10^{10}$ K. After ~ 100 yr (typical time of thermal relaxation), the star's interior (densities $\rho > 10^{10}$ g cm $^{-3}$) becomes nearly isothermal, and the energy balance of the cooling neutron star is determined by the following equation (e.g., Glen & Sutherland 1980):

$$C(T_i) \frac{dT_i}{dt} = -L_\nu(T_i) - L_\gamma(T_s) + \sum_k H_k ,$$

where T_i and T_s are the internal and surface temperatures, $C(T_i)$ is the heat capacity of the neutron star. Neutron star cooling thus means a decrease of thermal energy, which is mainly stored in the stellar core, due to energy loss by neutrinos from the interior ($L_\nu = \int Q_\nu dV$, Q_ν is the neutrino emissivity) plus energy loss by thermal photons from the surface ($L_\gamma = 4\pi R^2 \sigma T_s^4$). The relationship between T_s and T_i is determined by the thermal insulation of the outer envelope ($\rho < 10^{10}$ g cm $^{-3}$), where the temperature gradient is formed. The results of model calculations, assuming that the outer envelope is composed of iron, can be fitted with a simple relation (Gudmundsson, Pethick & Epstein 1983)

$$T_s = 3.1 (g/10^{14} \text{ cm s}^{-2})^{1/4} (T_i/10^9 \text{ K})^{0.549} \text{ MK},$$

where g is the gravitational acceleration at the neutron star surface, 1 MK = 1×10^6 K. The cooling rate might be reduced by heating mechanisms H_k , like frictional heating of superfluid neutrons in the inner neutron star crust or some exothermal nuclear reactions.

Neutrino emission from the neutron star interior is the dominant cooling process for at least the first 10^5 years. After $\sim 10^6$ years, photon emission from the neutron star surface takes over as the main cooling mechanism. Thermal evolution of a neutron star after the age of $\sim 10 - 100$ yr, when the neutron star has cooled down to $T_s = 1.5 - 3$ MK, can follow two different scenarios, depending on the still poorly known properties of super-dense matter (see Fig.8.4). According to the so-called *standard cooling scenario*, the temperature decreases gradually, down to $\sim 0.3 - 1$ MK, by the end of the neutrino cooling era and then falls down exponentially, becoming lower than ~ 0.1 MK in $\sim 10^7$ yr. In this scenario, the main neutrino generation processes are the modified Urca reactions, $n+N \rightarrow p+N+e+\bar{\nu}_e$ and $p+N+e \rightarrow n+N+\nu_e$, where N is a nucleon (neutron or proton) needed to conserve momentum of reacting particles. In the *accelerated cooling scenarios*, associated with higher central densities (up to 10^{15} g cm $^{-3}$) and/or exotic interior composition (e.g., pion condensation, quark-gluon plasma), a sharp drop of temperature, down to $0.3 - 0.5$ MK, occurs at an age of $\sim 10 - 100$ yr, followed by a more gradual decrease, down to the same ~ 0.1 MK at $\sim 10^7$ yr. The faster cooling is caused by the direct Urca reactions, $n \rightarrow p + e + \bar{\nu}_e$ and $p + e \rightarrow n + \nu_e$, allowed at very high densities (Lattimer et al. 1991). An example of standard and accelerated cooling curves is shown in Figure 8.4. The neutron star models used in these calculations are based on a ‘‘moderate’’ equation of state which opens the direct Urca process for $M > 1.35M_\odot$; the stars with lower M undergo the standard cooling. Recent studies have shown that both the standard and accelerated cooling can be substantially affected by nucleon superfluidity in the stellar interiors (see Tsuruta 1998 and Yakovlev, Levenfish & Shibantov 1999 for comprehensive reviews). In particular, there can exist many cooling curves intermediate between those of the standard and accelerated scenarios, depending on properties of nucleon superfluidity, which are also poorly known.

Thus, the thermal evolution of neutron stars between ~ 10 and $\sim 10^6$ yr is very sensitive to the composition and structure of their interiors, in particular, to the equation of state at super-nuclear densities. Therefore, measuring surface temperatures of neutron stars is an important tool to study the super-dense matter. Since typical temperatures of such neutron stars correspond to the extreme UV – soft X-ray range, the thermal radiation from cooling neutron stars can be observed with X-ray detectors sufficiently sensitive at $E \lesssim 1$ keV.

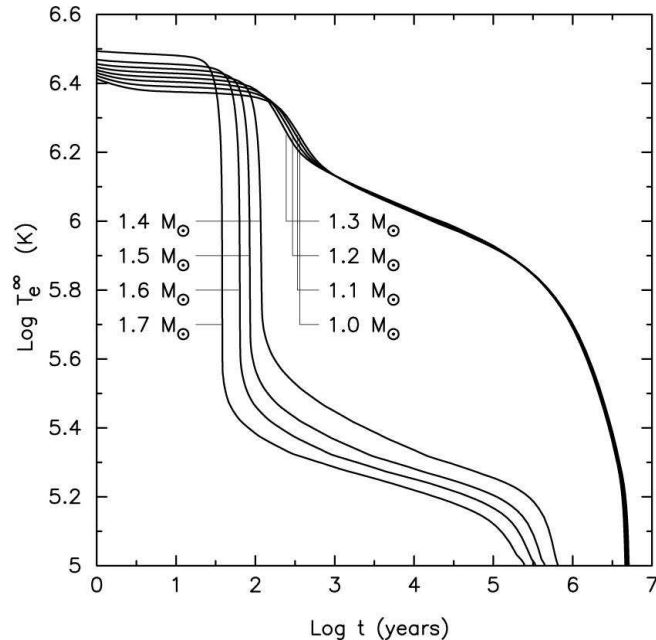


Figure 8.4: Fast cooling vs. standard cooling for neutron stars with different masses. T_e^∞ is the effective surface temperature as observed at infinity (i.e. the gravitational redshift is taken into account), t is the age. Stars of higher masses have a very high core density such that the direct Urca reactions (e.g., direct beta decay) are allowed. This causes a higher neutrino emissivity and hence a faster energy loss (more efficient cooling) by neutrino emission. The sharp temperature drop at an age of 50 – 100 yrs represents the temperature inversion point. Here, the interior of the star, from which the neutrinos have escaped without interaction, is cooler than outer neutron star layers which causes the outer regions to heat up the inner parts of the star. (From Page & Applegate 1992).

8.2.2.3 Photospheric Emission from Cooling Neutron Stars

Thermal radiation has been observed from about a dozen isolated neutron stars. Much more detailed data on thermal radiation from these and other neutron stars are expected from the X-ray observatories Chandra and XMM-Newton. To interpret these observations, detailed and accurate models for spectra and light curves of thermal radiation from neutron stars are needed. Properties of the neutron star thermal radiation are determined, as in usual stars, by a thin, partially ionized atmosphere with temperature growing inward. As a result, the neutron star thermal radiation may be substantially different from blackbody radiation (Pavlov & Shibano 1978). Modeling of neutron star atmospheres requires a special approach because neutron stars possess very strong magnetic fields, $B \sim 10^{11} - 10^{13}$ G. In such fields the electron cyclotron energy, $E_{ce} = 11.6 (B/10^{12} \text{ G}) \text{ keV}$, strongly exceeds the thermal energy, $kT \sim 0.01 - 1 \text{ keV}$. As a result, the atmospheres are essentially anisotropic, so that the absorption and emission of photons depend on the direction of the photon wavevector, and the radiation propagates there as two normal (polarization) modes with nearly orthogonal polarizations and quite different opacities (Gnedin & Pavlov 1974; Bulik & Pavlov 1996). The energy dependences of these opacities are substantially different from each other and from the opacity at $B = 0$. Since the ratio β of the cyclotron energy to the Coulomb energy¹⁰ is very large, the structure of atoms and ions is distorted by the strong magnetic field, which changes the energies and strengths of spectral features and ionization equilibrium of the atmospheric plasma. As a result, the spectrum, angular distribution and polarization of thermal radiation depend on the magnetic field.

Another important effect is that the nonuniform magnetic field leads to a nonuniform surface temperature distribution because of anisotropic heat conduction (Greenstein & Hartke 1983; Shibano & Yakovlev 1996), which enhances pulsations of thermal radiation due to the neutron

¹⁰e.g., $\beta = E_{ce}/(Z^2 \text{Ry}) = 850 Z^{-2} (B/10^{12} \text{ G})$ for one-electron ions; Z is the ion charge, $\text{Ry} = me^4/(2\hbar^2) = 13.6 \text{ eV}$ is the ionization potential of the hydrogen atom.

star rotation. The high density of the atmospheric matter ($\sim 1 - 100 \text{ g cm}^{-3}$ at unit optical depth), caused by the immense gravitational acceleration, $g \sim 10^{14} - 10^{15} \text{ cm s}^{-2}$, poses additional complications. In particular, the non-ideality (pressure) effects lead to pressure ionization and smooth out the spectral dependences of the opacities. The huge surface gravity also leads to chemical stratification of neutron star atmospheres, so that upper layers, which determine the properties of the emitted radiation, are comprised of the lightest element present. This means, in particular, that if a neutron star has accreted some amount of hydrogen (e.g., from the circumstellar medium or from the envelope ejected during the supernova explosion), its radiative properties are determined by the hydrogen atmosphere.

A convenient approach to modeling of neutron star atmospheres was described by Pavlov et al. (1995). It includes, as for usual stars, solving of a set of equations for hydrostatic equilibrium, energy balance, ionization equilibrium, and radiative transfer, complemented by calculations of spectral opacities for partially ionized, nonideal plasma. For atmospheres with strong magnetic fields, two coupled equations of radiative transfer for the intensities of two polarization modes have to be solved. The input parameters for the modeling are the chemical composition, effective temperature T_{eff} (or total radiative flux $\propto T_{\text{eff}}^4$), magnetic field B (including the field orientation at the radiating neutron star surface), and gravitational acceleration g (or the neutron star mass M and radius R).

Low-field Neutron Star Atmospheres

It is commonly accepted that very old neutron stars, like the $10^8 - 10^{10}$ years old millisecond pulsars, have “low” surface magnetic fields, $B \sim 10^8 - 10^9 \text{ G}$, which do not affect the X-ray opacities of the atmospheric plasma at temperatures of interest (at $E_{ce} \ll E$, $E_{ce} \ll kT$, and $\beta \ll 1$). First models of the low-field neutron star atmospheres were calculated by Romani (1987). Further works (Rajagopal and Romani 1996; Zavlin, Pavlov, & Shibano 1996) used improved opacities (Iglesias and Rogers 1996) for pure hydrogen, helium and iron compositions. These works have shown that the spectra of radiation emerging from a light-element (H or He) atmosphere are much harder (less steep) than the blackbody spectra at $E \gtrsim kT_{\text{eff}}$ (see Fig. 8.5). The reason for such behavior is that the hydrogen and helium opacities decrease with increasing E , so that the radiation of higher energies is formed in deeper and hotter layers. As a result, fitting observed spectra with the standard blackbody model yields spectral (blackbody) temperatures exceeding the true effective temperatures by a factor of 1.5 – 3, which makes a great difference for the comparison with the models of neutron star cooling.

The spectra emitted from iron atmospheres are much more complex due to numerous spectral features produced by iron ions in various stages of ionization (see Fig. 8.5). Some of these features are observable even with moderate-resolution (e.g, CCD) spectrometers. On the other hand, when observed with very low energy resolution, the iron atmosphere spectra look very similar to the blackbody spectra.

The local specific intensity of radiation decreases with the angle between the neutron star surface and the wave vector, and the shape of the angular distribution depends on photon energy and chemical composition. This (limb-darkening) effect must be taken into account for fitting of both the spectra and the pulse profiles if the radiation is emitted from hot spots on the neutron star surface, like in millisecond pulsars (Pavlov & Zavlin 1997; Zavlin & Pavlov 1998).

High-field Neutron Star Atmospheres

First models of magnetic hydrogen atmospheres with $B \sim 10^{11} - 10^{13} \text{ G}$ have been constructed recently (Shibano et al. 1992; Pavlov et al. 1994, 1995; Zavlin et al. 1995a). These models are based upon simplified opacities of strongly magnetized, partially ionized hydrogen plasma. These opacities do not include the bound-bound transitions, neglect the motional Stark effect, and use a simplified model for the ionization equilibrium. Nevertheless, the models provide a qualitatively correct description for the magnetic effects on the emergent radiation, and they are accurate enough in the case of high effective temperatures, $\gtrsim 1 \text{ MK}$, when the hydrogen is almost completely ionized even in the very strong magnetic fields.

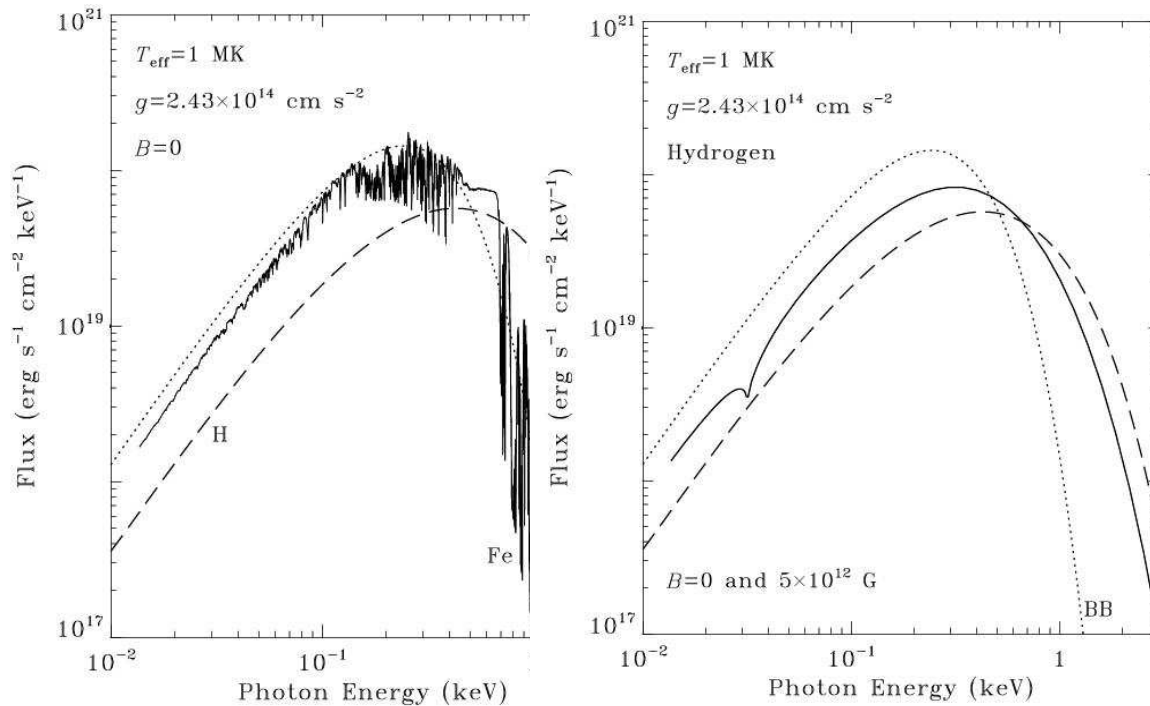


Figure 8.5: *Left*: Simulated spectra of hydrogen and iron neutron star atmospheres with low magnetic field, together with the blackbody spectrum, for $T_{\text{eff}} = 1$ MK. *Right*: The simulated spectra of hydrogen neutron star atmospheres with high and low magnetic fields (solid and dashed lines, respectively).

Since the magnetic atmospheres are much more transparent in the “extraordinary” polarization mode, whose opacity is strongly reduced by the magnetic field, very deep (hot and dense) layers are responsible for the observed radiation. Their X-ray spectra are harder than the blackbody spectrum at the same effective temperature, although not as much as the low-field spectra. The only spectral line in the spectra of completely ionized hydrogen atmospheres is the proton cyclotron line at the energy $E_{cp} = (m_e/m_p)E_{ce} = 6.3 (B/10^{12} \text{ G}) \text{ eV}$ (see Fig. 8.5). The spectra depend not only on strength, but also on direction of the magnetic field, which means that the radiative flux emitted by a rotating neutron star is pulsed even if the surface temperature is uniform. Angular distribution of the local intensity shows a sharp peak along the magnetic field and a broader peak at intermediate angles (the “pencil” and “fan” components), the widths of the peaks depend on photon energy. This means that the pulse profiles of radiation emitted from hot polar caps may be much sharper than those emitted from low-field atmospheres. The pulse shape strongly depends on the mass-to-radius ratio due to bending of photon trajectories in the strong gravitational fields (Zavlin, Shibano & Pavlov 1995b; Shibano et al. 1995). The radiation emitted from magnetic atmospheres is strongly polarized; the degree of polarization depends on E , B , and M/R (Pavlov & Zavlin 2000).

First results obtained with the improved hydrogen atmosphere models (Pavlov & Zavlin 2001), which include the bound-bound transitions, show that spectral lines, considerably broadened by the motional Stark effect (Pavlov & Mészáros 1993; Pavlov & Potekhin 1995), become prominent at $T_{\text{eff}} \lesssim 0.5$ MK. The strongest line is observed at $E \simeq \{75 [1 + 0.13 \ln(B/10^{13} \text{ G})] + 63 (B/10^{13} \text{ G})\} \text{ eV}$.

Magnetic iron atmosphere models have been considered by Rajagopal, Romani, & Miller (1997). Making use of the so-called adiabatic approximation ($\ln \beta \gg 1$), these authors calculated the energies and wave functions of the iron ions and the radiative opacities of the polarization modes. Although these models are inevitably rather crude, they provide a baseline for comparison with the magnetic hydrogen atmosphere models and for future work on heavy-element atmosphere modeling. Similar to the low-field case, the magnetic iron atmosphere spectra are fairly close to the blackbody spectra when observed with low-resolution detectors. Developing more accurate iron atmosphere models is important for adequate interpretation of future high-resolution X-ray observations of the neutron star thermal radiation.

8.3 The Current Picture of High-Energy Emission Properties of Isolated Neutron Stars

As a result of observations with the satellite observatories ROSAT, EUVE, ASCA, BeppoSAX, RXTE, CGRO, HST, Chandra and XMM-Newton, the number of rotation-powered pulsars seen at X-ray, gamma-ray and optical energies has increased substantially in the last decade of the century. For the first time it became possible to carry out multi-wavelength studies of the pulsar emission. This is a big advantage as the physical processes which cause the emission in different wavelength bands are obviously related to each other. Although the quality of the data obtained with different instruments is inevitably rather inhomogeneous, and the conclusions drawn on these data are therefore not fully certain in many cases, there is a general consensus that a first big step towards discrimination between different emission scenarios has been made. In this respect, even more is expected from the new observatories, Chandra and XMM-Newton, launched at the end of the century. Results from the first year of Chandra, which are briefly mentioned in this Section, seem to justify these high expectations.

8.3.1 Young Neutron Stars in Supernova Remnants

X-ray observations allow us to find both supernova remnants (SNRs) and the compact objects that may reside within them. In fact, neutron stars and neutron star candidates have been found in a small fraction, $< 10\%$, of the 220 known galactic SNRs (Green 1998; Kaspi 2000, and references therein). Less than half of these objects are radio pulsars, the others are radio-silent (or, at least, radio-quiet) neutron stars which are seen only in X-rays (some of them in gamma-rays). The young radio pulsars can be divided in two groups, Crab-like and Vela-like pulsars, according to somewhat different observational manifestations apparently associated with the evolution of pulsar properties with age. The radio-silent neutron stars include anomalous X-ray pulsars, soft gamma-ray repeaters, and “quiescent” neutron star candidates. We will briefly review all the groups in this subsection.

8.3.1.1 Crab-like Pulsars

It is well established that magnetospheric emission from charged particles, accelerated in the neutron star magnetosphere along the curved magnetic field lines, dominates the radiation from young *rotation-powered* pulsars with ages $\lesssim 5000$ years (cf. 8.2.2). In the case of the Crab pulsar at least $\sim 75\%$ of the total soft X-ray flux is emitted from the co-rotating magnetosphere (Becker & Trümper 1997). Accordingly, its radiation is characterized by a power-law spectrum¹¹, and its spin-modulated lightcurve exhibits two narrow peaks per period (see Fig. 8.6). The Crab pulsar is also a bright gamma-ray and optical-UV source. Its X-ray, gamma-ray, optical and radio pulsations are all phase-aligned, demonstrating that the emission in these bands is clearly non-thermal and originates from the same site in the pulsar magnetosphere. The slope of its flux spectrum slowly increases with photon energy — the photon index varies from $\alpha = 1.1$ at $E \sim 1$ eV to $\alpha = 2.1$ at $E \sim 10^{10}$ eV.

As the Crab pulsar is the youngest rotation-powered pulsar and thus should be the hottest neutron star, one could expect to observe its thermal surface emission at the off-pulse phases, when the thermal flux is not buried under the powerful magnetospheric emission. However, even the Einstein HRI and ROSAT HRI, despite their high angular resolution, were not able to completely get rid of a contribution from the compact synchrotron nebula around the pulsar (see Fig.8.7), so that only an upper limit on the thermal flux has been established from the DC level of the soft X-ray pulse profile. Becker & Aschenbach (1995) found an upper limit of about 2 MK for the surface temperature of the Crab pulsar from the ROSAT HRI observations, consistent with the predictions of standard cooling models.

¹¹The spectrum of the non-thermal radiation is a power-law, $dN/dE \propto E^{-\alpha}$, as the energy distribution of the particles which emit this radiation follows a power-law in a broad energy range.

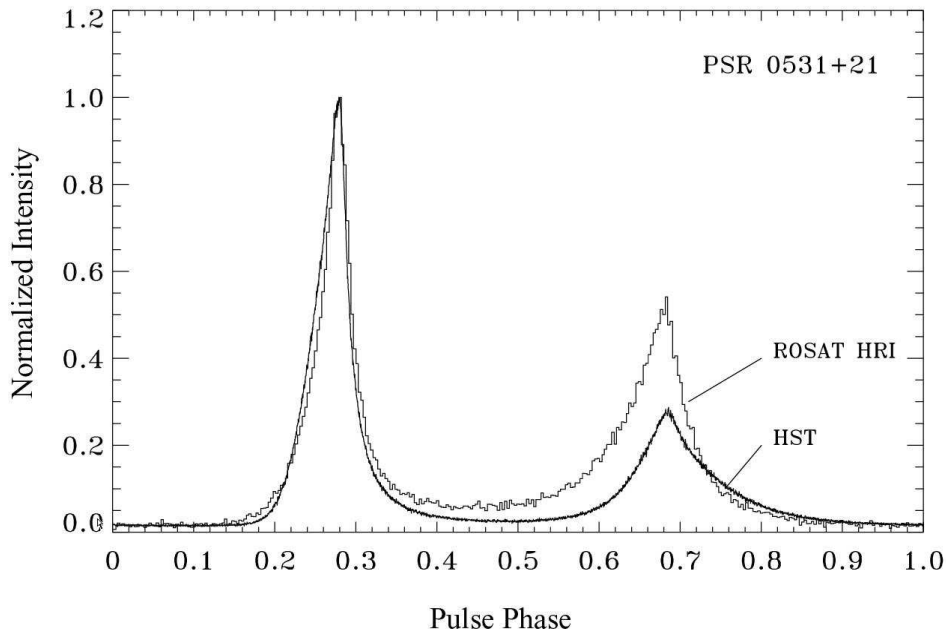


Figure 8.6: The Crab pulse profile as observed with HST and ROSAT in the optical and soft X-ray bands. Its characteristic double-peaked shape is observed at all wavelengths. The phase difference between the first and second peak shows a weak energy dependence.

The ROSAT HRI data taken from the Crab Nebula have been used to improve our understanding of this object in many aspects. Greiveldinger & Aschenbach (1999), using the HRI observations spanning a period of more than 6 years, have shown that the X-ray intensity of the inner synchrotron nebula varies on time scales of years by about 20%. The intensity variations are found to be confined to rather large ($\sim 25'' \times 25''$, or 0.25×0.25 pc) regions in the *torus* (its radius is ≈ 0.4 pc). Using the instruments aboard Chandra, it will be easy to further investigate these long-term variations. First images taken with the Advanced CCD Imaging Spectrometer (ACIS) aboard Chandra have already provided spectacular details of the inner nebula structure associated with the pulsar-wind outflow — in addition to the *torus* ($r \approx 0.38$ pc), the *inner ring* ($r \approx 0.14$ pc), *jet* and *counter-jet* have been identified (Weisskopf et al. 2000). To demonstrate the recent progress in X-ray astronomy, the images of the Crab pulsar and its plerion, as seen by the Chandra ACIS and the ROSAT HRI, are shown in Figure 8.7.

Emission properties similar to those found for the Crab pulsar are observed from the pulsars B0540–69, J0537–6909 and B1509–58 in the supernova remnants N158A, N157B and MSH 15–52 (the former two are in the Large Magellanic Cloud). In particular, PSR B0540–69 has a compact X-ray nebula strongly resembling that around the Crab pulsar, and $\approx 40\%$ of the pulsar’s soft X-ray photons are pulsed (Seward & Harnden 1994; Gotthelf & Wang 2000). This pulsar has been detected in optical (Boyd et al. 1995; Hill et al. 1997) but not in gamma-rays. Like for the Crab-pulsar, its optical pulse profile is very similar to the profile observed at X-ray energies (Gouiffes, Finley & Ögelman 1992; Mineo et al. 1999).

PSR B1509–58 has the highest period derivative among the known pulsars. Optical radiation from this pulsar has not yet been detected, and only upper limits have been obtained for its gamma-radiation above ~ 10 – 30 MeV, suggesting a break in the gamma-ray spectrum somewhere between 10 and 100 MeV (Kuiper et al. 1999). Its X-ray emission in the ROSAT band is found to have a pulsed fraction of about 65% (Becker & Trümper 1997). The soft X-ray pulse is phase-aligned with the hard X-ray and gamma-ray pulses detected by the CGRO detectors BATSE, OSSE and COMPTEL up to at least 10 MeV (Ulmer et al. 1994; Kuiper et al. 1999). These high-energy pulses appear phase-shifted by ~ 0.3 periods relative to the radio pulse. Based on

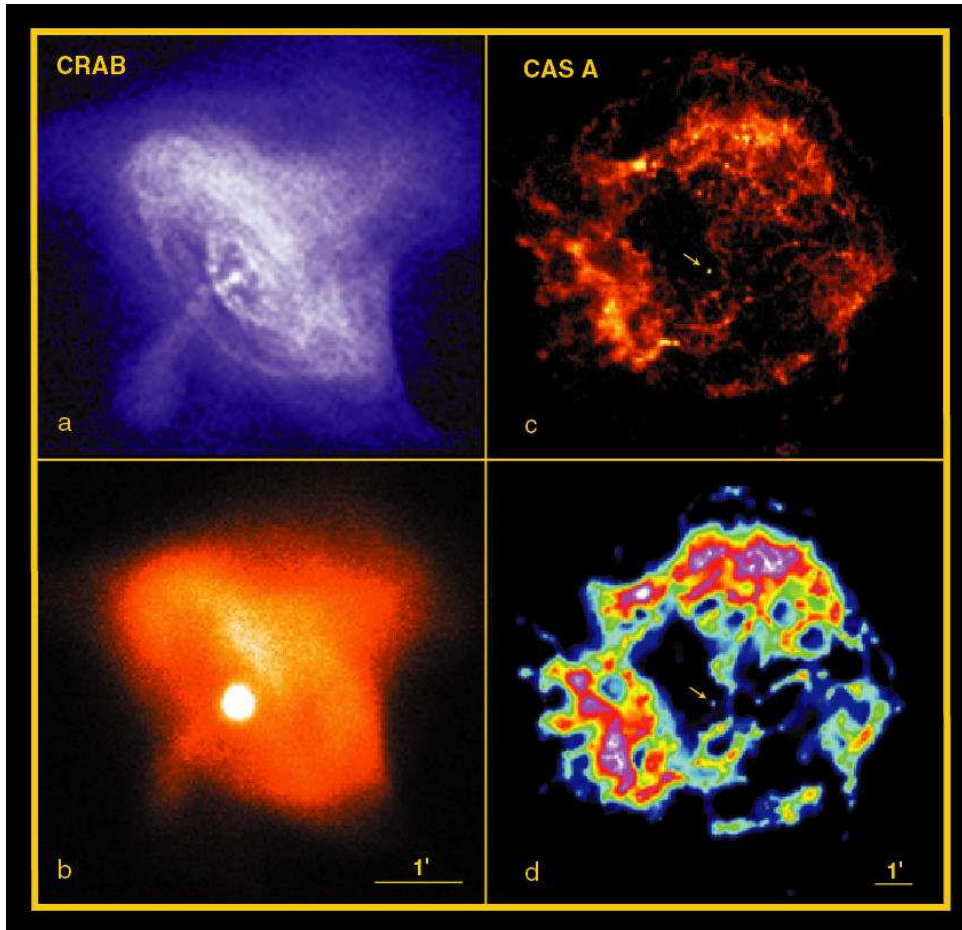


Figure 8.7: The Crab as observed with the Chandra ACIS (a) and the ROSAT HRI (b). The images demonstrate the improvement of angular resolution between the two detectors by a factor of 10. In the Chandra image much more details of the pulsar-driven nebula become visible. Image (c) shows another recent discovery made by Chandra: the point source close to the geometrical center of Cassiopeia A (Cas A), a very young (320 yr) supernova remnant. The corresponding ROSAT HRI image is shown in (d). Only the unprecedented high spatial resolution provided by Chandra allowed one to detect the point source, a young neutron star or a black hole, identified *a posteriori* in deep Einstein HRI and ROSAT HRI images.

the ROSAT HRI observations, Brazier & Becker (1997) have proposed that the X-ray nebula surrounding PSR 1509–58 (see Fig. 8.8) is comprised of a *torus* and a *jet*, similar to the Crab synchrotron nebula. A nearby region of enhanced X-ray emission, RCW 89, may be caused by the collision of the collimated pulsar wind with the outer shell of the supernova remnant.

PSR J0537–6909 has been discovered recently (Marshall et al. 1998) with RXTE and ASCA and later detected with ROSAT (Wang & Gotthelf 1998). It is particularly interesting due to its very short period of 16 ms, the shortest one among the “regular” pulsars, despite the fact that it is older ($\tau \sim 5000$ yr) than the other three members of this subclass of pulsars. The ROSAT HRI image shows a bright X-ray nebula whose size (≈ 2 pc) and cometary shape indicate that the pulsar is moving with a supersonic velocity, ~ 1000 km/s, and the X-ray emission of the nebula originates mainly from a bow shock.

Thus, all the very young pulsars show strong non-thermal X-ray emission with an X-ray luminosity $L_x \sim 10^{34} - 10^{36}$ erg s $^{-1}$ in the ROSAT energy range, and they are surrounded by pulsar-powered nebulae (plerions) and supernova ejecta. Presumably, their magnetospheric emission extends from at least infrared to gamma-ray energies, with typical photon indices varying

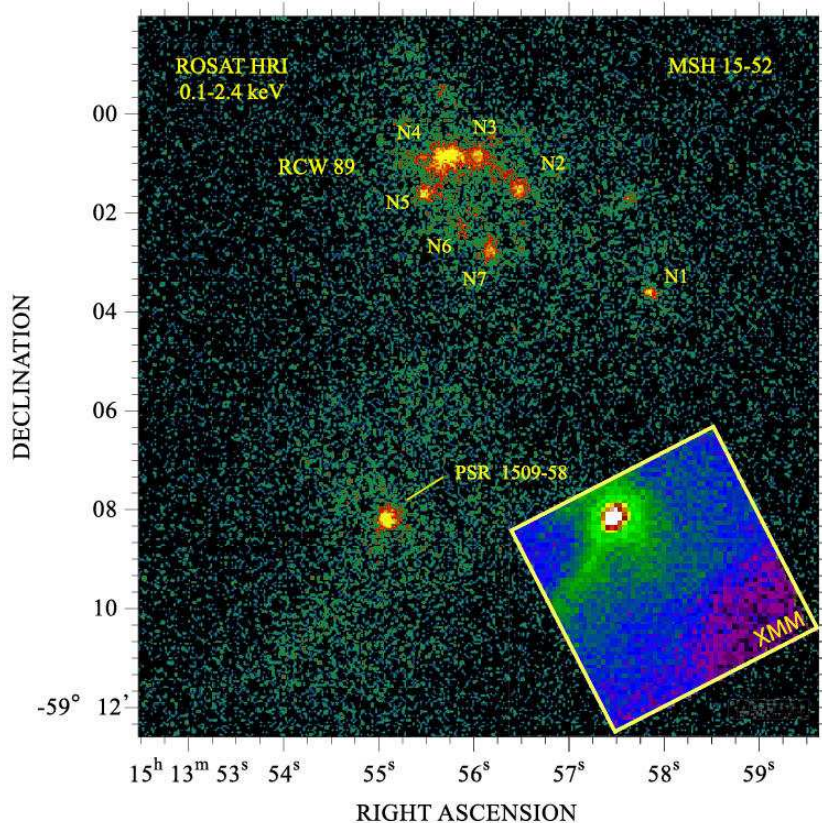


Figure 8.8: Soft X-ray image of MSH 15–52 and RCW 89 as seen by the ROSAT HRI. The most striking features are the compact knots in RCW 89 (only the brightest seven are labeled, N1–N7), the point source at the location of PSR B1509–58, the synchrotron nebula around PSR B1509–58, and the extended diffuse emission in RCW 89. The inset shows a $4' \times 4'$ area around the pulsar as seen by the PN-Camera aboard XMM-Newton.

between ≈ 1 and ≈ 2 (about 1.4 – 1.7 in the soft X-ray range).

8.3.1.2 Vela-like pulsars

Pulsars with a spin-down age of $\sim 10^4 - 10^5$ years are often referred to as Vela-like pulsars, because of their apparent similar emission properties. About ten pulsars of this group have been detected in X-rays (cf. Tab. 8.2), four of them (the Vela pulsar B0833–45, PSR B1706–44, B1046–58 and B1951+32) are gamma-ray pulsars, and only the Vela pulsar has been detected in the optical band. In some respects, these objects appear to be different from the Crab-like pulsars. In particular, their pulses at different energies are not phase-aligned with each other, their optical radiation is very faint compared to that of the very young pulsars, and the overall shape of their high-energy spectra looks different. For instance, the closest ($d \approx 300$ pc) and, hence, best-investigated Vela pulsar (see Fig. 8.9 and Fig. 8.10) has an optical luminosity four orders of magnitude lower than the Crab pulsar (Manchester et al. 1978; Nasuti et al. 1997), whereas its rotation energy loss is only a factor of 65 lower. Its light curve shows two peaks in the gamma-ray range (Kanbach et al. 1994) and at least three peaks in the X-ray range (Strickman et al. 1999; Pavlov et al. 2000a), versus one peak at radio frequencies, whose phase does not coincide with any of the high-energy pulses. The pulsed fraction in the soft X-ray range, $\approx 12\%$, is much lower than that observed from the Crab-like pulsars.

In contrast to the young Crab-like pulsars, the soft X-ray spectrum of the Vela pulsar has a substantial thermal contribution with an apparent temperature of ≈ 1 MK (Ögelman, Finley &

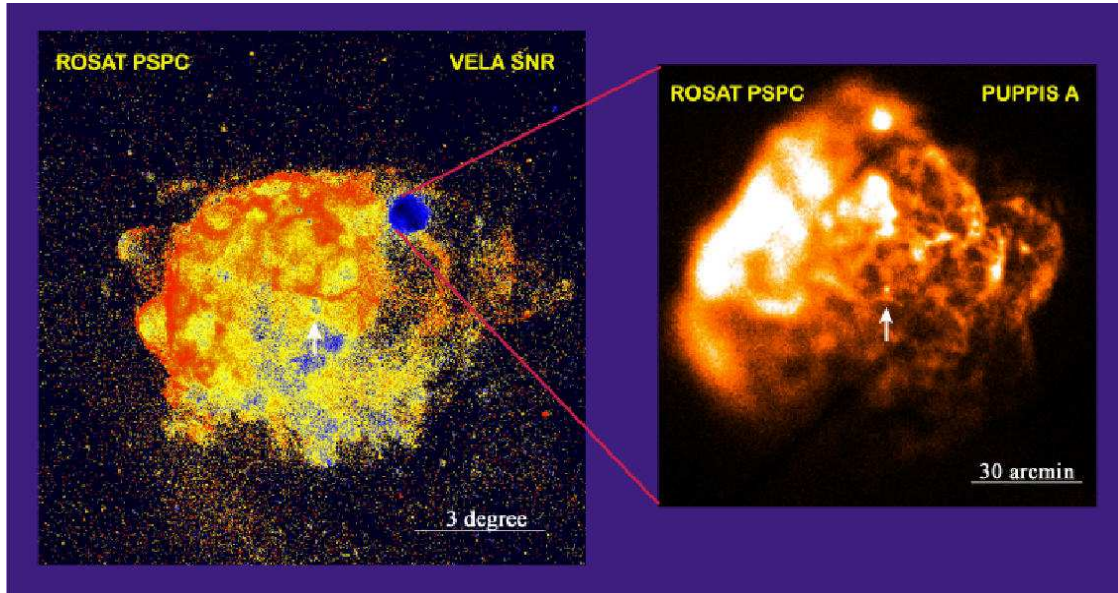


Figure 8.9: *Left*: ROSAT PSPC image of the Vela SNR. Different colors here correspond to different energies of X-ray photons, from red (lower energies) to blue (higher energies). The location of the Vela pulsar is indicated by the arrow. *Right*: Zoomed image of the Puppis A SNR, located at the North-West edge of the Vela remnant. The arrow indicates the point source RX J0820–4300 which is a very good candidate for a young cooling neutron star showing photospheric emission (see 8.3.1.3).

Zimmerman 1993; Page, Shibano & Zavlin 1996). On the other hand, the spatial structure of the Vela plerion strongly resembles the inner Crab nebula — it also has a torus-like structure, an inner ring and jets (cf. Fig. 8.7a/b and Fig. 8.10). The symmetry axis of the nebula, which can be interpreted as the projection of the pulsar’s rotation axis onto the sky plane, is co-aligned with the direction of proper motion, exactly as for the Crab pulsar, which indicates that the “natal kick” of the neutron star occurs along the rotation axis of the neutron star progenitor. The idea of torus configuration formed by a shock-confined pulsar wind was first introduced by Aschenbach & Brinkmann (1975) as a model to explain the shape of the inner Crab nebula. The discovery of a similar torus-like structure in the Vela synchrotron nebula hints that this model may be applicable to many young pulsars. According to this model, the torus-like structure and its geometrical orientation with respect to the direction of the pulsar’s proper motion arise because the interaction of the post-shock plasma with the ambient medium compresses the plasma and amplifies the magnetic field ahead of the moving pulsar. This, in turn, leads to enhanced synchrotron emission with the observed torus-like shape.

Typical sizes of the X-ray nebula structures scale approximately as $\dot{E}^{1/2}$, as one should expect for relativistic pulsar winds shocked by an ambient medium (Rees & Gunn 1974). For instance, the inner ring radii for the Crab and Vela nebulae are 0.14 pc (for $d = 2$ kpc) and 0.02 pc (for $d = 300$ pc), whereas the full extents of the X-ray nebulae are 1 pc and 0.1 pc, respectively. The X-ray luminosity of the Vela plerion is only 0.04% (0.1–2.4 keV) of the pulsar’s spin-down energy loss, versus 5%, 13% and 1% for the Crab, B0540–69 and B1509–58 X-ray nebulae, respectively.

Since the other pulsars of this subclass are at much larger distances, it is hard to resolve them from the putative surrounding X-ray nebulae. Therefore, what has been observed is mainly emission from a pulsar-powered synchrotron nebula combined with a small contribution of magnetospheric or thermal radiation. The latter is expected to dominate at soft X-ray energies, below 0.5–1 keV, hardly observable in distant pulsars because of interstellar absorption. The relatively small contribution of the pulsar’s radiation, perhaps with intrinsically low pulsed fraction, has precluded the detection of pulsed soft X-ray emission from these objects. Compact X-ray nebulae of physical sizes $\sim 0.3(d/2.4 \text{ kpc})$ pc, $0.4(d/4 \text{ kpc})$ pc and $0.7(d/2.5 \text{ kpc})$ pc have been observed

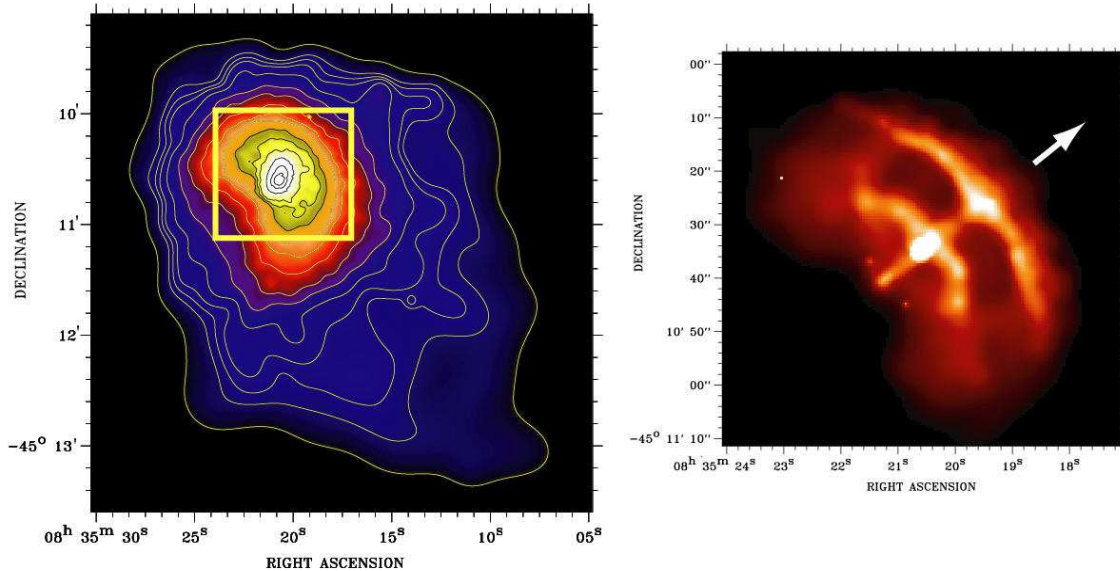


Figure 8.10: The Vela pulsar and its X-ray plerion as observed with the ROSAT HRI (a) and Chandra ACIS (b). In both images, the pulsar is the brightest source. The Chandra image shows the spatially resolved inner part of the plerion, corresponding to the central yellow box in the ROSAT image. The arrow indicates the direction of the pulsar proper motion which is aligned with the rotation axis.

from PSR B1706–44 (Becker, Brazier & Trümper 1995; Finley et al. 1998), B1823–13 (Finley, Srinivasan & Park 1996), and B1951+32 (Safi-Harb, Ögelman & Finley 1995), respectively. These sizes exceed that of the Vela X-ray nebula, despite close values of \dot{E} , which can be tentatively explained by lower pressure of the ambient medium around these pulsars. It is also possible that future Chandra observations will reveal a fine spatial structure of these nebulae, which would lead to the explanation of the apparent difference with the compact nebula around the prototype Vela pulsar.

Thus, in spite of the apparent differences between the Crab-like and Vela-like pulsars, the sample of well-investigated objects is still too scarce to determine whether these differences are caused by a general evolution of pulsar properties during the first millenia of their lives or whether they are due to some incidental properties inherent to the pulsars or their surroundings (for instance, different orientations of the magnetic and rotation axes, or different properties of the ambient medium). The most critical for understanding the nature of these objects will be Chandra observations with high angular resolution, as these observations will allow us to resolve the pulsars from their X-ray plerions.

8.3.1.3 Radio-silent Neutron Stars in Supernova Remnants

X-ray images of some young SNRs show bright point sources which have not been detected in radio, optical and gamma-ray bands (see Table 8.1). The youngest among the detected sources of this type is the point source in the very young (320 yr) Cassiopeia A supernova remnant (cf. Fig. 8.7). This source was discovered in the first light Chandra observation (Tananbaum 1999) and subsequently found in archival Einstein HRI and ROSAT HRI images (Aschenbach 1999; Pavlov & Zavlin 1999). The true nature of this source remains elusive (Pavlov et al. 2000b). It shows no long-term (20 yr) or short-term (days, months) variability, and no X-ray pulsations have been detected in the available data. The observed spectra do not have enough counts to distinguish between different simple spectral models (e.g., power-law or blackbody, corresponding to a non-thermal or thermal origin of the detected emission). However, it turns out that the spectrum is much softer than those of young radio pulsars. If the emission occurs from the neutron

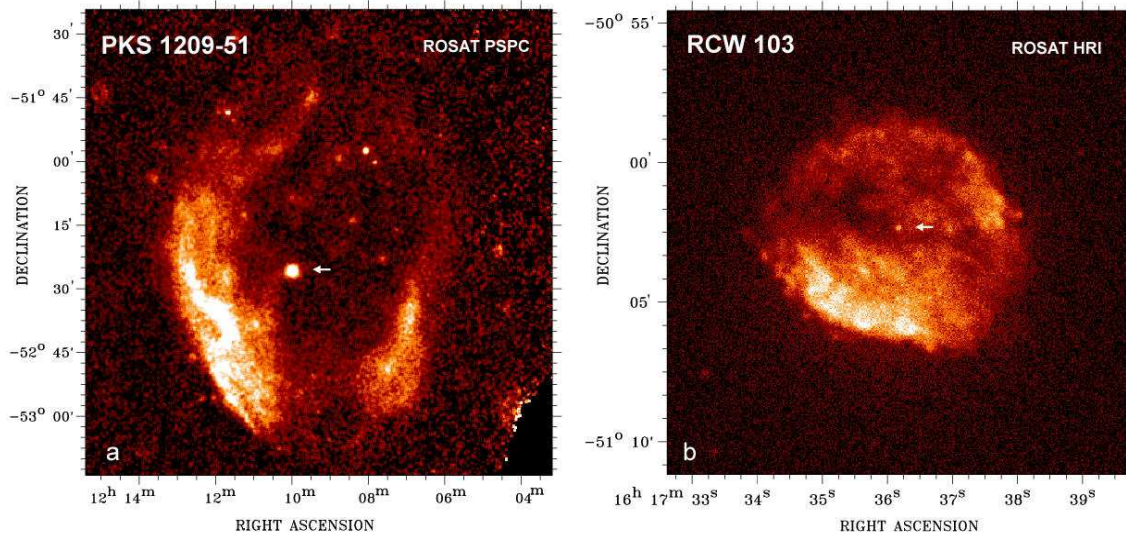


Figure 8.11: ROSAT images of the supernova remnants PKS 1209–51/52 and RCW 103. The arrows indicate the positions of the neutron star 1E 1207–5209 and the neutron star candidate 1E 161348–5055. Note the different scales of the images. PKS 1209-51/52 has an extent of about 1.5° whereas the size of RCW 103 is about $10'$.

star surface, the temperature distribution over the surface has to be strongly non-uniform. The blackbody fit gives a temperature of 7 MK and a radius of the emitting region of 0.3 km. Assuming that there are magnetically confined hydrogen or helium hot polar caps on a cooler iron surface, Pavlov et al. (2000b) obtained 2.8 MK and 1 km for the cap temperature and radius, and 1.7 MK for the surface effective temperature. This anisotropic temperature distribution can cause a spin-modulation of the X-ray flux, which remains to be detected in future observations.

A similar point source, 1E 1207–5209 at the center of the ≈ 7 -kyr-old remnant PKS 1209–51/52 (see Fig. 8.11), was discovered with HEAO-1 (Tuohy et al. 1979) and studied with Einstein, EXOSAT, ROSAT and ASCA (Helfand & Becker 1984; Kellett et al. 1987; Mereghetti, Bignami & Caraveo 1996). Its X-ray spectrum suggests that the X-rays are emitted from a hydrogen or helium atmosphere of the neutron star, having an effective temperature 1.2 – 1.3 MK (Zavlin, Pavlov & Trümper 1998). The analysis of the Chandra observation of this source has shown that its X-ray flux is modulated with a 424 ms period (Zavlin et al. 2000), which finally proves that it is indeed a neutron star.

Another example of the radio-silent neutron star candidate is 1E 161348–5055 at the center of the supernova remnant RCW 103. This source was discovered with the Einstein Observatory (Tuohy & Garmire 1980) and has an estimated age of 1 – 3 kyr. Its X-ray spectrum very strongly resembles that of the Cas A central point source. However, comparing two ASCA observations of RCW 103, Gotthelf, Petre & Vasisht (1999a) found an order-of-magnitude decrease in its luminosity in four years, which hints that this object may be an accreting source. Even more puzzling is the six-hour periodicity of its flux reported by Garmire et al. (2000) from the Chandra observations and archival ASCA data. Further investigations of 1E 161348–5055 with Chandra and XMM-Newton are underway and will resolve the true nature of this source.

Similar to the previous examples is the point source in Puppis A (cf. Fig. 8.9), a supernova remnant located at the edge of the Vela remnant. Puppis A has an age of about 4 kyr and harbors a central radio-silent X-ray bright source, RX J0822–4300, which is supposed to be a neutron star candidate (Petre, Becker & Winkler 1996). Contrary to the compact stellar remnants in Cas A and RCW 103, its spectrum and luminosity can be interpreted as emitted from the entire surface of a neutron star with a 10 km radius and a temperature of 1.6 – 1.9 MK, assuming that the surface is covered by a hydrogen or helium atmosphere (Zavlin, Trümper & Pavlov 1999). This temperature, like that inferred for 1E 1207–5209, is compatible with standard neutron star

cooling models. It is worth noting that fitting the spectrum with a blackbody model gives an improbably small neutron star radius of 1.0 – 1.5 km and a higher temperature 4 – 5 MK.

From what we know so far about radio-silent neutron stars in supernova remnants, one can conclude that such sources are quite different from radio pulsars (in particular, they do not show any activity inherent to radio pulsars). On the other hand, it is very plausible that, in fact, they are more common than radio pulsars, and the relatively small number of the discovered members of this class is due to observational selection — it is much easier to detect and identify active pulsars than these “quiet” sources observable only in the soft X-ray band.

For completeness, we should also mention a number of young SNRs whose central parts show bright extended (plerion-like) X-ray sources with centrally-peaked emission, with properties strongly resembling those observed from the plerions around Crab-like pulsars, but without a point source detected. Typical examples of this class are 3C58 and G21.5–0.9, with estimated ages of 800 yr and ~ 1 kyr (Helfand, Becker & White 1995; Slane et al. 2000). It seems very plausible that these SNRs do have active pulsars at the centers of their plerions, but an unfavorable direction of the pulsar beam precludes detection of pulsations.

8.3.1.4 Anomalous X-ray Pulsars and Soft Gamma-Ray Repeaters

In addition to the above-discussed young, X-ray-bright and radio-quiet neutron star candidates which do not show strong pulsations, a number of apparently young neutron stars with strong X-ray pulsations, the so-called *anomalous X-ray pulsars* (AXPs) and *soft gamma-ray repeaters* (SGRs), have been discovered recently (see Table 8.1 for references). At least some of them are believed to be associated with supernova remnants. A common property of these objects is that their periods are in a narrow range of 5 – 12 s, substantially exceeding typical periods of radio pulsars. The AXPs and SGRs are, however, strongly different in their gamma-ray activity. While no gamma-ray emission has been detected from AXPs, SGRs emit occasional gamma-ray bursts of enormous energy, up to 10^{42} – 10^{44} erg.

Six anomalous X-ray pulsars have been discovered by the end of the century (see Table 8.1). They form a homogeneous class of pulsating neutron stars, clearly different from both the accreting pulsars in X-ray binaries and rotation-powered radio pulsars (Mereghetti 2000). AXPs show a relatively stable period evolution with $\dot{P} \approx (0.05\text{--}4) \times 10^{-11} \text{ s s}^{-1}$. Characteristic spin-down ages $\tau \sim 3 - 100$ kyr and magnetic fields $B \sim 10^{14}$ – 10^{16} G were estimated under the assumption that the spin-down is due to magneto-dipole braking, which is not necessarily correct because these objects are not powered by their rotation. If the estimated magnetic field strengths are correct, they strongly exceed those of radio pulsars, so that it has been suggested that AXPs, as well as SGRs, are *magnetars* — neutron stars with superstrong magnetic fields (Thompson & Duncan 1995, 1996). They have soft X-ray spectra, with characteristic blackbody temperatures $T \approx 4 - 7$ MK and/or power-law indices $\alpha \approx 2.5 - 4$, and typical luminosities $L_x \sim 10^{34} - 10^{36} \text{ erg s}^{-1}$. Typical blackbody areas are 1 – 2 orders of magnitude smaller than the NS surface area. At least three AXPs are associated with supernova remnants (see Table 8.1).

AXPs have been studied with many X-ray observatories, but their nature remains elusive. Although it has been widely accepted that these objects are magnetars, no direct proof of their superstrong magnetic fields has been obtained. It is not clear whether their X-ray emission indeed originates from the neutron star surface or from the magnetosphere and/or from a synchrotron nebula, and whether it is due to “internal” radiation mechanisms (thermal or magnetospheric emission) or due to accretion from, e.g., a residual disk (van Paradijs, Taam & van den Heuvel 1995). Observations with Chandra and XMM, however, will probably provide the answer.

Soft gamma-ray repeaters (SGRs) are among the most fascinating galactic objects. After the discovery of periods in the range of $P = 5 - 8$ s and period derivatives $\dot{P} \sim 10^{-10} \text{ s s}^{-1}$ (in two of the four known SGRs), it has been suggested that these sources are associated with young, $\sim 1 - 10$ kyr, neutron stars in supernova remnants. The energy released during the most powerful bursts of these sources is enormous — e.g., an energy of $\gtrsim 10^{44}$ erg was estimated for the August 27, 1998 outburst of SGR 1900+14 (Inan et al. 1999).

SGRs are not only extremely powerful sources of gamma-ray bursts, but also bright quiescent

Object	P/f_p s/%	\dot{P} 10^{-11}	Age kyr	d kpc	N_H 10^{21} cm $^{-2}$	$T_{bb}/R_{bb}/f_{bb}$ MK/km/%	α	L_x 10^{33} erg s $^{-1}$	optical	SNR	Ref.
NSCs in SNRs:											1
CXO J2323+5848	.../< 35	...	0.3	3.4	8–15	7/0.3	3.2	2	R> 25	Cas A	2
1E 1613–5055	21,000/60(?)	...	1–3	3.3	4–10	6/0.5	~ 4	1–10 ^v	R> 24	RCW 103	3
RX J0820–4300	.../< 15	...	4	2.2	3–6	4/1	4.8	8	R> 24	Pup A	4
1E 1207.4–5209	0.42/10	...	3–20	~ 2	1–2	3/1.2	5.2	5	V> 23	G296.5+10.0	5
RX J0002+6246	0.24/10(?)	...	~ 20	~ 3	~ 4	2/3	> 4	2	V> 18	G117.7+0.6(?)	6
AXPs:											7
1E 1048–5937	6.45/70	~ 3	~ 3	~ 5	5	7/1/55	2.5	20 ^v	V> 20	...	8
1E 1841–045	11.77/35	4	2–4	7	30	–	3.4	400	...	Kes 73	9
1RXS J1708–4009	11.00/30	1.9	9	8	14	5/3/17	2.9	~ 1000	R> 17	...	10
1E 2259+586	6.98/30	0.048	3–20	~ 6	10	5/4/40	3.9	~ 100 ^v	R> 25	G109.1–1.0	11
4U 0142+61	8.69/10	0.2	60	1–5	10	5/2.4/40	~ 4	80	V> 24	...	12
AX J1845.0–0300	6.97/50	...	< 8	8–15	46	8/1.5	–	50 ^v	...	G29.6+0.1	13
SGRs											
SGR 0526–66	8/...	...	~ 0.5(?)	55	0.5	...	3.5	1000	V> 21	N49 in LMC	14
SGR 1806–20	7.48/15	~ 10	1–10	~ 15	60	...	2.2	400	K= 8.4(?)	G10.0–0.3(?)	15
SGR 1900+14	5.16/10	~ 10	~ 10	~ 7	10–20	6/1/20	1.5	60	J> 18	G42.8+0.6	16
SGR 1627–41	~ 5	11(?)	80	...	2.5	50	...	G337.0–0.1(?)	17
Isolated NSCs:											18
RX J1856.5–3754	.../< 10	...	1000(?)	< 0.1	0.1–0.2	0.7/< 20	–	< 0.5	V= 25.7	–	19
RX J0720.4–3125	8.39/10	< 0.08	...	< 0.5	0.1–0.2	0.9/< 20	–	< 0.6	B= 26.5(?)	–	20
RX J0420.0–5022	22.7/40(?)	~ 0.2	0.7/...	–	...	B> 25	–	21
RX J0806.4–4123	0.2–0.3	0.9/...	–	...	B> 24	–	22
RX J1605.3+3549	~ 0.1	1.2/...	–	...	B> 26	–	23
RX J1308.6+2127	5.15/20	1.347	< 10	0.5–1.5	0.21	1.02–1.08/..	–	0.41	B> 26	–	24

Table 1: List of observational properties of the X-ray detected radio-quiet neutron star candidates (NSCs). The individual columns are as follows: 1– object (AXPs = anomalous X-ray pulsars, SGRs = soft gamma-ray repeaters); 2– period and pulsed fraction; 3– period derivative in s s $^{-1}$; 4– age estimated as $P/(2\dot{P})$ if the period and its derivative are known, or as SNR age if the NSC is associated with SNR; 5– distance estimate; 6– hydrogen column density; 7– temperature and radius for a blackbody fit; f_{bb} , where present, is the fraction of the blackbody flux in a blackbody+power-law fit; 8– photon power-law index; 9– characteristic X-ray luminosity (persistent luminosity for SGRs; ^v marks variable sources); 10– optical magnitudes or limits; 11– host SNRs; 12– *References*: 1– Caraveo et al. (1996); Kaspi (2000); Brazier & Johnston (1999); 2– Pavlov et al. (2000b); Chakrabarty et al. (2001); 3– Gotthelf et al. (1997); Gotthelf et al. (1999a); Garmire et al. (2000); 4– Petre et al. (1996); Zavlin et al. (1999); 5– Mereghetti et al. (1996); Zavlin et al. (1998); Zavlin et al. (2000); 6– Hailey & Craig (1995); 7– Mereghetti & Stella (1995); van Paradijs et al. (1995); Mereghetti (2000); 8– Seward et al. (1986); Oosterbroek et al. (1998); 9– Vasisht & Gotthelf (1997); Gotthelf et al. (1999b); 10– Sugizaki et al. (1997); Israel et al. (1999a); Kaspi et al. (1999); 11– Gregory & Fahlman (1980); Corbet et al. (1995); Rho & Petre (1997); Hulleman et al. (2000); 12– Israel et al. (1994); White et al. (1996); Wilson et al. (1999); Israel et al. (1999b); 13– Torii et al. (1998); Gotthelf & Vasisht (1998); Gaensler et al. (1999); 14– Mazets et al. (1979a); Rothschild et al. (1994); Danner et al. (1998); 15– Kulkarni & Frail (1993); Sonobe et al. (1994); Fenimore et al. (1994); van Kerkwijk et al. (1995); Corbel et al. (1997); Kouveliotou et al. (1998); Hurley et al. (1999a); Mazets et al. (1979b); 16– Hurley et al. (1999b); Murakami et al. (1999); Israel et al. (1999); Woods et al. (1999a); Marsden et al. (1999); Woods et al. (1999b); Woods et al. (1999c); 17– Woods et al. (1999d); Corbel et al. (1999); Hurley et al. (2000); 18 – Neuhäuser & Trümper (1999); 19– Walter et al. (1996); Pavlov et al. (1996b); Walter & Matthews (1997); Walter et al. (2000); 20– Haberl et al. (1997); Motch & Haberl (1998); Kulkarni & van Kerkwijk (1998); 21– Haberl et al. (1999); 22– Haberl et al. (1998); 23– Motch et al. (1999); 24– Schwope et al. (1999), Hambarian et al. (2001)

Characteristics of the optical, X-ray and gamma-ray detected rotation-powered pulsars.

Pulsar	Comment	detected						$\dot{E}/(4\pi d^2)$	$\log \dot{E}$	$\log L_x^{tot}$	$\log L_x^{puls}$	$\log L_x^n$	$\log L_{bol}^\infty$	$\log (P/2\dot{P})$	P	$\dot{P} \times 10^{-15}$	d	$\log B_\perp$
		R	O	X _s	X _h	γ _s	γ _h	erg/s/cm ²	erg/s	erg/s	erg/s	erg/s	erg/s	years	ms	s s ⁻¹	kpc	Gauss
B0531 + 21	Crab	p	p	p	p	p	$9.3 \cdot 10^{-7}$	38.65	35.98	35.85	37.3	≤ 34.1	3.10	33.40	420.96	2.00	12.58	
B0833 - 45	Vela	p	p	p	p	p	$2.3 \cdot 10^{-7}$	36.84	32.25	31.25	32.95	~ 32.3	4.05	89.29	124.68	0.30	12.53	
J0205 + 6449	in 3C58	-	-	p	-	-	$3.2 \cdot 10^{-8}$	37.42	32.20		34.31		3.73	65.67	193.52	2.60	12.55	
J2229 + 6114	in G106.6+2.9	p	-	p	-	d	$2.0 \cdot 10^{-8}$	37.34	33.01				4.02	51.62	78.27	≥ 3	12.30	
J1617 - 5055	near RCW 103	p	-	p	-	-	$1.3 \cdot 10^{-8}$	37.20					3.91	69.33	136.05	3.30	12.49	
B0633 + 17	Geminga	p	p	p	-	p	$1.1 \cdot 10^{-8}$	34.51	31.10	30.62		31.2	5.53	237.09	10.97	0.16	12.21	
B1706 - 44	in G343.1-02.3	p	-	d	-	p	$8.6 \cdot 10^{-9}$	36.53	33.15			≤ 33.5	4.24	102.45	93.04	1.82	12.49	
B1509 - 58	in MSH 15-52	p	-	p	p	p	$7.7 \cdot 10^{-9}$	37.25	34.29	34.10	35.3	≤ 33.9	3.19	150.23	1540.19	4.30	13.19	
B1951 + 32	in CTB 80	p	-	d	-	p	$5.0 \cdot 10^{-9}$	36.57	33.44		34.0	≤ 33.9	5.03	39.53	5.85	2.50	11.69	
J1811 - 1926	in G11.2-0.3	-	-	p	-	-	$2.4 \cdot 10^{-9}$	36.80					4.38	64.67	44.00	≥ 5	12.23	
B1046 - 58	Vela twin	p	-	d	-	p	$1.9 \cdot 10^{-9}$	36.30	≤ 32.11			≤ 32.7	4.31	123.65	95.92	2.98	12.54	
B1259 - 63*	Be-star/bin	p	-	d	d	d	$1.7 \cdot 10^{-9}$	35.92	32.95			≤ 33.8	5.52	47.76	2.27	2.00	11.51	
J0537 - 6909	in N157B/LMC	p	-	p	-	-	$1.6 \cdot 10^{-9}$	38.68					3.71	16.11	51.24	49.4	11.96	
B1823 - 13	Vela like	p	-	d	-	-	$1.4 \cdot 10^{-9}$	36.45	33.39			≤ 33.9	4.33	101.45	74.95	4.12	12.45	
B1800 - 21	G8.7-0.1	p	-	d	-	-	$1.2 \cdot 10^{-9}$	36.35	33.06			≤ 33.8	4.30	133.61	134.32	3.94	12.63	
B1929 + 10		p	d	p	-	-	$1.1 \cdot 10^{-9}$	33.59	30.00	29.5		≤ 31.4	6.49	226.51	1.16	0.17	11.71	
J0437 - 4715	ms-PSR	p	-	p	-	-	$1.0 \cdot 10^{-9}$	33.62	30.86	30.3		≤ 31.2	9.50	5.75	$2.0 \cdot 10^{-5}$	0.18	8.54	
B1937 + 21	ms-PSR	p	-	p	-	-	$7.1 \cdot 10^{-10}$	36.04	≤ 32.10				8.37	1.55	$1.0 \cdot 10^{-4}$	3.60	8.61	
B1821 - 24	ms-PSR, in M28	p	-	p	p	-	$6.2 \cdot 10^{-10}$	36.35	33.24			≤ 33.7	7.48	3.05	$1.6 \cdot 10^{-3}$	5.50	9.35	
B0656 + 14	cooling NS	p	p	p	-	?	$5.5 \cdot 10^{-10}$	34.58	32.98	32.15		32.9	5.05	384.87	55.03	0.76	12.67	
J0030 + 0451	ms-PSR	p	-	p	-	-	$5.4 \cdot 10^{-10}$	33.53	30.10				9.88	4.86	$1.0 \cdot 10^{-5}$	0.23	8.32	
B0540 - 69	in N158A, LMC	p	p	p	p	-	$5.1 \cdot 10^{-10}$	38.17	36.21	36.1	37.2	≤ 36.1	3.22	50.37	479.06	49.4	12.70	
J2124 - 3358	ms-PSR	p	-	p	-	-	$4.7 \cdot 10^{-10}$	33.55	30.35	29.8		≤ 31.1	9.86	4.93	$1.08 \cdot 10^{-5}$	0.25	8.36	
J1105 - 6107		p	-	d	-	-	$4.3 \cdot 10^{-10}$	36.40					4.80	63.19	15.80	7.00	12.00	
B1957 + 20	ms-PSR	p	-	d	-	-	$4.1 \cdot 10^{-10}$	35.06	31.93			≤ 32.9	9.32	1.60	$1.2 \cdot 10^{-5}$	1.53	8.14	
J1024 - 0719	ms-PSR	p	-	d	-	-	$3.6 \cdot 10^{-10}$	33.72	29.48				9.76	5.18	$1.8 \cdot 10^{-5}$	0.35	8.49	
B0950 + 08		p	?	d	-	-	$3.3 \cdot 10^{-10}$	32.75	29.35			≤ 31.0	7.24	253.06	0.23	0.12	11.39	
J1744 - 1134	ms-PSR	p	-	d	-	-	$2.4 \cdot 10^{-10}$	33.28	29.30				9.86	4.07	$0.86 \cdot 10^{-5}$	0.26	8.27	
B1610 - 50		p	-	d	-	-	$2.5 \cdot 10^{-10}$	36.20					3.87	231.60	492.54	7.26	13.03	
J0538 + 2817	in G180.0-1.7	p	-	d	-	-	$1.3 \cdot 10^{-10}$	34.69	32.74			≤ 33.6	5.79	143.15	3.66	1.50	11.87	
J1012 + 5307	ms-PSR	p	-	d	-	-	$1.2 \cdot 10^{-10}$	33.60	30.20			≤ 30.8	9.76	5.25	$1.4 \cdot 10^{-5}$	0.52	8.45	
B1055 - 52	cooling NS	p	d	p	-	p	$1.1 \cdot 10^{-10}$	34.48	33.42	32.57		33.5	5.73	197.10	5.83	1.53	12.03	
B0355 + 54		p	-	d	-	-	$8.8 \cdot 10^{-11}$	34.66	31.96			≤ 33.8	5.75	156.38	4.39	2.07	11.92	
B2334 + 61	G114.3+0.3	p	-	d	-	-	$8.6 \cdot 10^{-11}$	34.79	31.86			≤ 33.4	4.61	495.24	191.91	2.46	12.99	
J0218 + 4232	ms-PSR	p	-	p	-	-	$6.5 \cdot 10^{-11}$	35.37	32.75			≤ 33.1	8.66	2.32	$8.0 \cdot 10^{-5}$	5.85	8.63	
B0823 + 26		p	-	d	-	-	$2.6 \cdot 10^{-11}$	32.66	29.83			≤ 31.0	6.69	530.66	1.72	0.38	11.99	
J0751 + 1807	ms-PSR	p	-	d	-	-	$1.5 \cdot 10^{-11}$	33.88	31.60			≤ 32.2	9.84	3.47	$8.0 \cdot 10^{-6}$	2.02	8.23	

Table 2. List of rotation-powered pulsars that have been detected in the radio, optical, X- and γ -ray wavebands, ordered according to their spin-down flux density at Earth $\dot{E}/4\pi d^2$. The individual columns are as follows: 1. Pulsar name; 3-8. Energy ranges in which pulsed (p), unpulsed (d) radiation has been detected: R – radio, O – optical, X_s – soft X-rays ($E_\gamma \sim 1\text{keV}$), X_h – hard X-rays ($E_\gamma \sim 10\text{keV}$), γ_s – soft γ -rays ($E_\gamma \sim 1\text{MeV}$) and γ_h – hard γ -rays ($E_\gamma > 100\text{MeV}$). Possible detections are indicated by a question mark. \dot{E} is the pulsar spin-down power $I\Omega\dot{\Omega}$; L_x^{tot} the sum of the pulsed and unpulsed X-ray luminosities assuming isotropic emission. L_x^{puls} is the pulsed luminosity; L_x^n is the total X-ray luminosity including synchrotron nebula emission. All luminosities L_x are calculated for the ROSAT energy range 0.1 – 2.4 keV. For Geminga, PSR 0656+14 and 1055-52 thermal and non-thermal contributions are included. L_{bol}^∞ is the bolometric luminosity. The upper limits have been computed for a neutron star with a medium stiff equation of state (FP-Model, $M = 1.4 M_\odot$ and $R = 10.85 \text{ km}$). *PSR 1259-63 was observed $\sim 13^\circ$ post-apastron. For references see Becker & Trümper (1997; 1999). Radio pulsar parameters have been taken from Taylor et al. (1995). Proper motion corrected period derivatives have been used for all those pulsars for which this effect is of significance and has been measured. A summary of the optical and γ -ray observations can be found in Caraveo (1995) and Thompson (1996), respectively.

X-ray sources, with typical luminosities $L_x \sim 10^{34} - 10^{36}$ erg s⁻¹. The origin of the quiescent radiation remains unclear. Statistically acceptable fits of the quiescent spectra can be obtained with a combined blackbody plus power-law model, with typical parameters $T \sim 5$ MK, $R \sim 1$ km and a photon-index of $\alpha = 1 - 4$. The blackbody component might be interpreted as thermal radiation from the neutron star surface, but the area of the emitting region is two orders of magnitude smaller than the neutron star surface area. The power-law component might hint that ultra-relativistic particles are involved, but no models have been suggested to explain their origin and acceleration mechanisms. However, with the poor angular resolution of the ASCA telescopes, it is difficult to separate the point source radiation from the diffuse SNR radiation, whereas the ROSAT count rates are too low for a precise spectral analysis. Chandra and XMM-Newton observations will yield much more definitive results and will allow one to reveal the nature of the quiescent emission from SGRs and to elucidate the properties of the ultra-magnetized neutron stars apparently responsible for their radiation.

8.3.2 Thermal Emission from Middle-Aged Pulsars

As we have discussed above, soft X-ray radiation of rotation-powered pulsars in an age interval of $\sim 10^5 - 10^6$ yrs should be dominated by thermal emission from the neutron star surface. These pulsars are old enough for their magnetospheric emission to become fainter than the thermal surface emission, but they are still young and hot enough to be detectable in the soft X-ray range. There are three middle-aged pulsars, Geminga, PSR B0656+14 and B1055-52, from which thermal X-ray radiation from the surface of the cooling neutron star has certainly been observed. Because of the similarity of their emission properties, they were dubbed *the three Musketeers* (Becker & Trümper 1997). The high-energy (IR through gamma-ray) spectra of these pulsars consist of two components. The thermal component dominates in the UV through soft X-ray range (up to 1 - 2 keV), whereas the non-thermal component with approximately power-law (PL) spectrum prevails in IR, optical, hard X-ray and gamma-ray ranges. It follows from the ROSAT and ASCA observations of the brightest middle-aged pulsar B0656+14 that the thermal component cannot be described by a single temperature, i.e. the neutron star surface temperature is not uniform (Greiveldinger et al. 1996; Zavlin, Pavlov & Halpern 2001). In the simplest model, the thermal component is comprised of a soft thermal component (TS) from most of the neutron star surface (at $E \lesssim 0.5 - 1$ keV) and a hard thermal component (TH) from polar caps heated by relativistic particles. An example of a TS+TH+PL fit to the IR-optical-X-ray spectrum of PSR B0656+14 is shown in Fig. 8.12. Alternatively, the temperature non-uniformity can be due to anisotropic heat conductivity of the neutron star crust caused by anisotropic magnetic field — the heat flux across the field is suppressed so that the magnetic poles are hotter than the equator (Greenstein & Hartke 1983).

The other two pulsars are not so bright as B0656+14, and their thermal components can be fitted with a single-temperature model (see Fig. 8.13 for the X-ray spectrum of Geminga).

The existence of at least two spectral components is also confirmed by a phase-resolved analysis of the X-ray emission (Ögelman 1995). All the three pulsars show a phase shift of $\sim 100^\circ$ at an energy 0.4 - 0.6 keV, accompanied by an increase in the pulsed fraction from $\sim 10 - 30\%$ to $\sim 20 - 65\%$. The X-ray pulse profiles for both the thermal and non-thermal components are found to be approximately sinusoidal. The weak modulation of the thermal soft component can be explained by the above-mentioned non-uniformity of the surface temperature due to the presence of a strong magnetic field. The surface temperatures of the three pulsars, obtained from blackbody fits, are in the range $T \sim 0.3 - 1.2$ MK. The radii of the emitting areas cannot be found without knowing the distances to these objects. Adopting the distances estimated from the radio-pulsar dispersion measure (which may be off by a factor of ~ 2), the radii are in the range $R \sim 7 - 30$ km, in rough agreement with the canonical neutron star radius of 10 km. The hard X-ray spectral components, dominating at energies above $\sim 1 - 2$ keV, can be interpreted as magnetospheric emission (Halpern & Wang 1997; Wang et al. 1998; Greiveldinger et al. 1996; Zavlin et al. 2001).

It should be stressed that the inferred effective temperatures, and hence the radius-to-distance

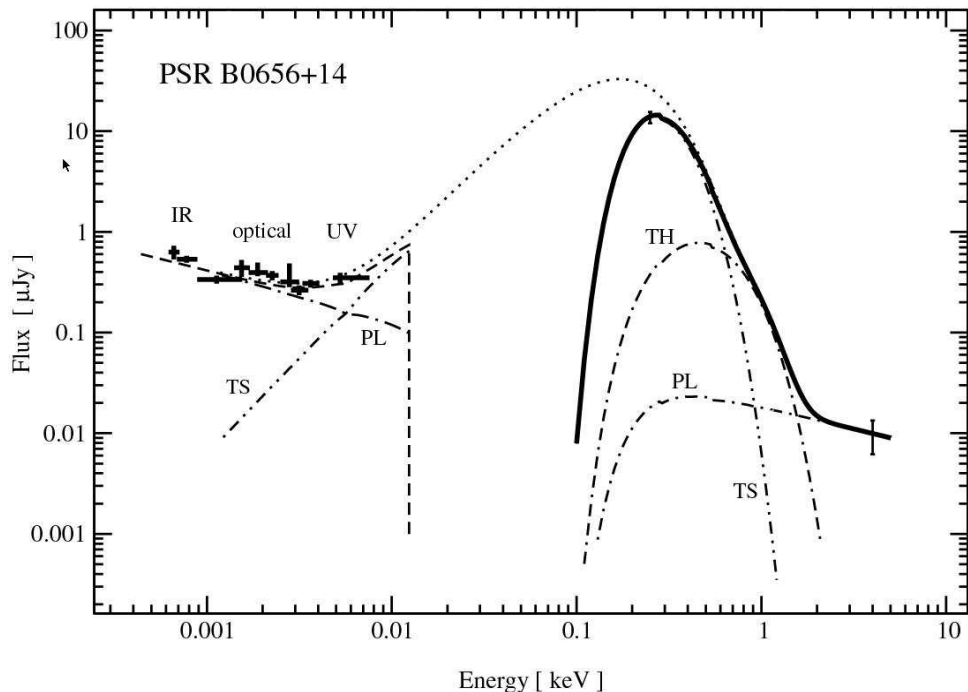


Figure 8.12: Energy spectrum of PSR B0656+14, a prototype middle-aged pulsar with thermal radiation dominating in soft X-rays. Shown are the X-ray (ROSAT and ASCA) spectrum fitted with a model consisting of thermal soft (TS), thermal hard (TH) and power-law (PL) components, and IR-optical-UV fluxes measured with the HST and ground-based telescopes. The error bars in the X-ray range show typical uncertainties in the ROSAT and ASCA bands. The dashed and dotted lines show the continuation of the X-ray spectrum to the optical band with and without allowance for interstellar absorption.

ratios, depend on the model of thermal component. For instance, if one assumes that the neutron star surface is covered by a hydrogen or helium atmosphere, the effective temperatures are lower than those derived from the simple blackbody fits by a factor of 1.5–3 (Pavlov et al. 1995; see also Section 8.2.2.3). An example demonstrating the difference of the temperatures inferred for the blackbody and hydrogen atmosphere model fits is shown in Figure 8.14. We see that the different spectral models correspond to quite different cooling scenarios and, hence, to different properties of the neutron star interiors. Heavy-element atmospheres give temperatures close to the blackbody temperatures. However, the heavy-element atmosphere spectra should show numerous absorption lines and photoionization edges (Rajagopal & Romani 1996; Zavlin et al. 1996). Because of low energy resolution of the ROSAT PSPC and low sensitivity of the ASCA SIS in soft X-rays, it has been impossible to detect such lines and thus to determine the chemical composition of neutron star atmospheres. We hope that this problem will be solved with Chandra and XMM-Newton. Without knowing the surface chemical composition, any conclusions about the effective temperatures and radii should be considered with caution.

Important information on the emission mechanisms of middle-aged pulsars can be obtained from observations in the optical and gamma-ray ranges. PSR B0656+14 and Geminga have been observed at near-IR, optical and near-UV frequencies (Pavlov et al. 1996a; Bignami et al. 1996; Shearer et al. 1996; Pavlov, Welty & Córdova 1997; Koptsevich et al. 2000), and PSR B1055–52 has been detected in a near-UV band (Mignani, Caraveo & Bignami 1997). For all the three pulsars, the IR-optical flux is clearly non-thermal, while the thermal component starts to dominate at UV frequencies (see an example in Fig. 8.12). For Geminga, a broad optical emission feature at $\sim 6000 \text{ \AA}$ was reported by Bignami et al. (1996), who attributed it to proton cyclotron emission from an atmospheric plasma. This interpretation does not look plausible because it requires an artificial velocity distribution for atmospheric electrons to explain the lack of electron cyclotron

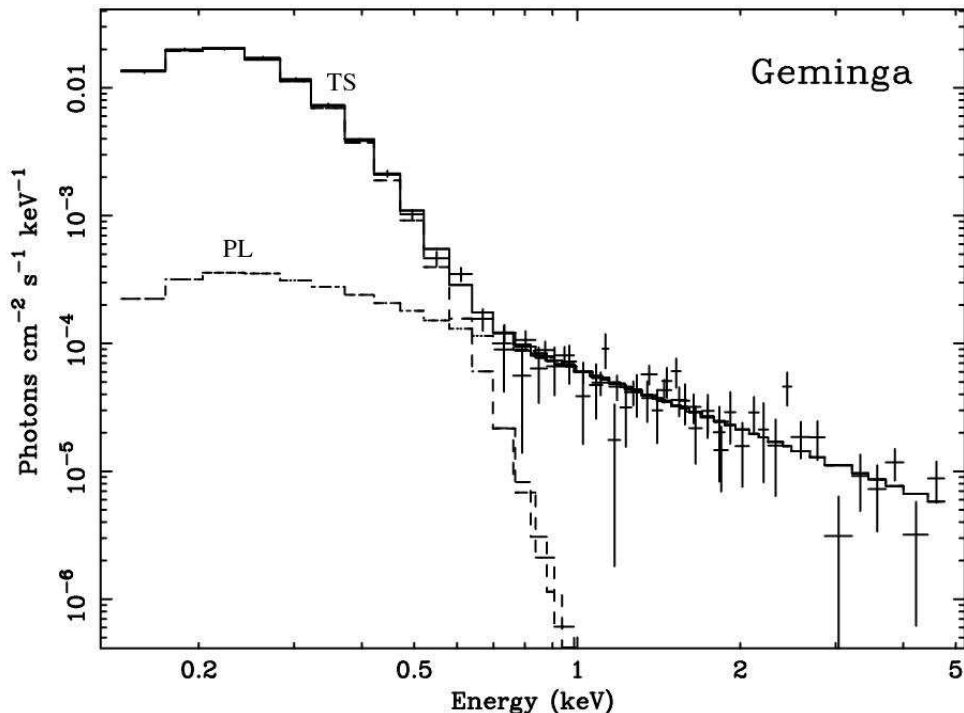


Figure 8.13: X-ray spectrum of Geminga — a typical spectrum of a middle-aged pulsar, consisting of a thermal component interpreted as emission from the neutron star surface, and a harder power-law (non-thermal) component, dominating beyond ≈ 0.7 keV. The soft part of the spectrum was obtained with ROSAT whereas the harder emission was observed by ASCA. (From Halpern & Wang 1997.)

line in the hard X-ray spectrum. The nature of this feature, and the overall optical spectrum of Geminga, can hardly be understood without spectroscopic observations (Martin, Halpern & Schiminovich 1998).

The two older middle-aged pulsars, Geminga and B1055–52, are bright gamma-ray pulsars in the CGRO EGRET energy range, 30 MeV – 20 GeV, which gives the main contribution to their photon luminosity (see Thompson et al. 1999, and references therein). Gamma-ray emission from B0656+14 has been marginally detected, at a 3σ level (Ramanamurthy et al. 1996). The gamma-ray spectra are close to power-laws, with photon indices of about 1.4 – 1.8 (see Fig. 8.16). A spectral turnover at about 3 GeV has been observed in the Geminga spectrum. The data can be interpreted with both the polar cap and outer gap models (see Section 8.2.2.1). Observations in a broader energy range with more sensitive gamma-ray detectors are required to construct a detailed model of the gamma-radiation.

Since all active pulsars are powerful sources of relativistic winds, one should expect that they generate pulsar-wind nebulae (PWNe), similar to those observed around the Crab-like and Vela-like pulsars. The PWN sizes should scale as $(\dot{E}/p_0)^{1/2}$, where p_0 is the pressure of the ambient medium. The existence of X-ray bright PWNe (albeit of much larger sizes) around several pulsars, including the three musketeers, was reported by Kawai & Tamura (1996) based on ASCA observations. However, the analysis of the ROSAT and BeppoSAX observations of these sources by Becker et al. (1999) did not confirm the ASCA results — the extended emission observed with ASCA was resolved in a number of unrelated background objects. In particular, Geminga and PSR B0656+14 are located in the Monogem ring (see Fig. 8.15), a $\sim 20^\circ$ wide object which is believed to be an old and nearby supernova remnant (see Plucinsky et al. 1996). A large fraction of the sources detected by ASCA are found to be diffuse and fuzzy emission of a small part of the Monogem ring rather than pulsar-powered nebulae.

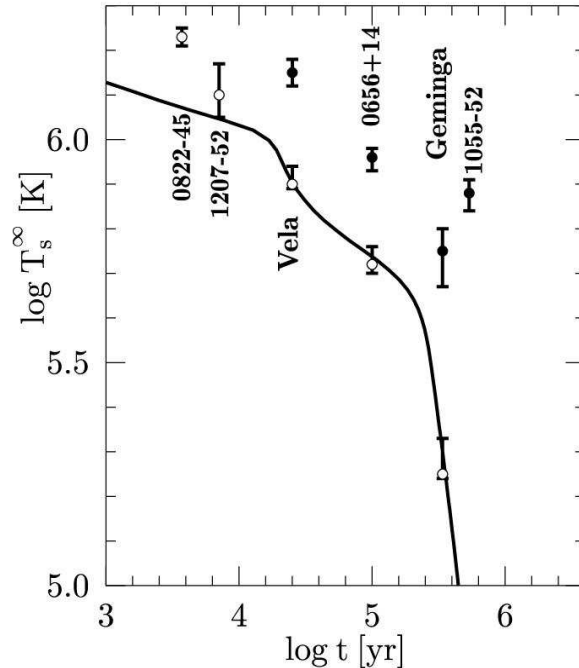


Figure 8.14: Surface temperatures for the three musketeers (PSR B0656+14, Geminga and B1055–52), the Vela pulsar and the radio-quiet neutrons stars RX J0822–4300 and 1E 1207–52. The hatched regions indicate the possible ranges of T_s^∞ as predicted by the standard (double hatched) and accelerated (single hatched) cooling models for different critical temperatures of the superfluid neutrons and protons, T_{cn} and T_{cp} ($\sim 10^6 - 10^{10}$ K). The solid line shows the standard cooling curve for a $1.30M_\odot$ neutron star with $T_{cn} = 200$ MK, $T_{cp} = 130$ MK. Filled and open circles indicate temperatures obtained from the blackbody and hydrogen-atmosphere fits, respectively. (From Yakovlev et al. 1999).

In addition to PSR B0656+14, B1055–52 and Geminga, one could expect thermal radiation from the cooling neutron star surface to dominate in soft X-ray emission from two more middle-aged pulsars detected with ROSAT, PSR B0538+28 and B0355+54. Both have spin parameters similar to those observed for Geminga and B1055–52, and both appear to be good candidates for gamma-ray pulsars. However, these sources are approximately a factor of 10 more distant than Geminga, so that the limited photon statistics has hampered a spectral or temporal analysis.

8.3.3 Old Nearby Radio Pulsars

When the age of a neutron star reaches $\sim 10^6$ yr, its temperature becomes too low to be observed in X-rays. At the same time, the energy loss rate \dot{E} , and hence the luminosity of non-thermal radiation and thermal radiation from polar caps of radio pulsars, also decrease with age. Therefore, old pulsars are faint in the X-ray range and can be observed only at small distances. ROSAT and ASCA have detected X-ray emission from three old and close pulsars: PSR B1929+10, B0950+08 and B0823+26. All the three are characterized by a spin-down age of 2 – 30 Myr and are at distances of $\sim 0.2 - 0.4$ kpc. Temporal and spectral information, however, is only available for PSR B1929+10 (Yancopoulos, Hamilton & Helfand 1994), whereas for the other two pulsars the sensitivity of ROSAT and ASCA was not sufficient to collect enough photons for a detailed analysis. The pulse profile of PSR B1929+10 is very broad, with a single pulse stretching across almost the entire phase cycle. Becker & Trümper (1997) and Wang & Halpern (1997) found that both the power-law and black-body models fit the observed spectrum equally well, leaving the origin of the detected X-rays unconstrained. If the observed radiation is interpreted in terms of thermal emission from hot polar caps ($T \sim 3$ MK), the caps appear to be very small ($A \sim 100$ m²), and their X-ray luminosity is much lower than predicted by many polar cap heating models.

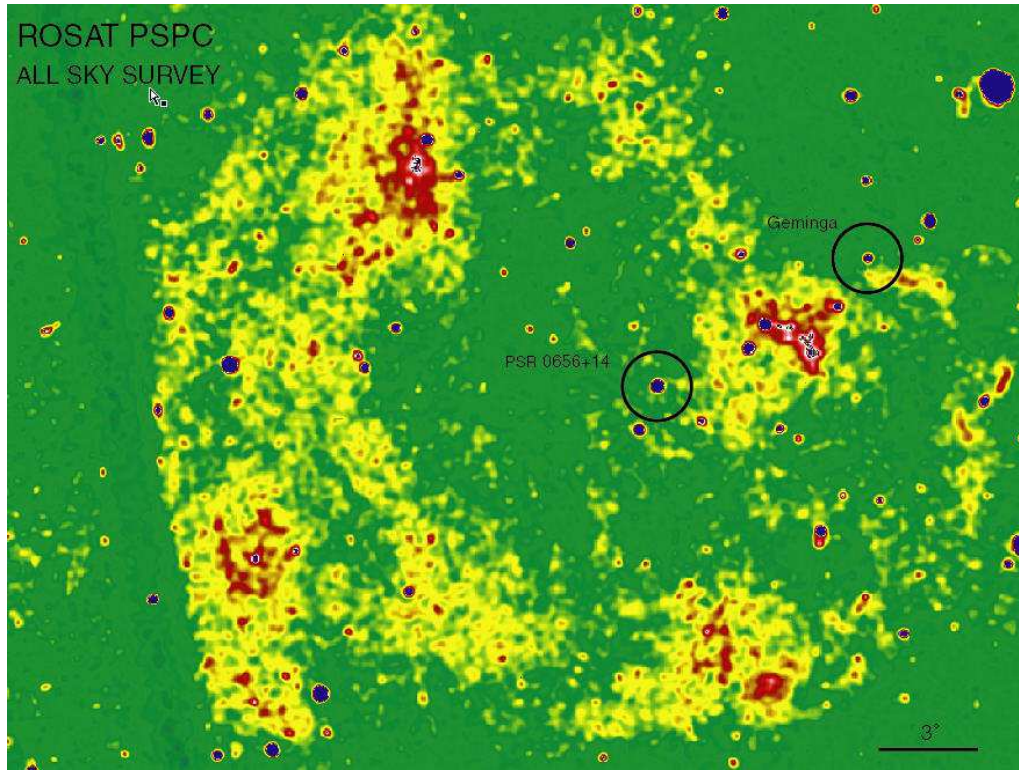


Figure 8.15: The 20° -wide Monogem Ring as observed in the ROSAT all-sky survey. The ROSAT PSPC full fields of view during the pointed observations of Geminga and PSR 0656+14 are indicated by circles. The image demonstrates that both pulsars are located in crowded regions with patchy background emission, strongly blurred with ASCA spatial resolution of $\sim 3'$. The image demonstrates the power of the first all-sky survey with an imaging X-ray telescope, providing X-ray images of extended celestial objects of very large sizes.

If this radiation is non-thermal, its luminosity is consistent with the general trend, $L_x \sim 10^{-3}\dot{E}$, found by Becker & Trümper (1997) for the non-thermal emission from those radio pulsars which are detected in the X-ray range (see Fig.8.17). The sensitivity of XMM-Newton and Chandra is required to finally identify the emission mechanism.

Although the thermal radiation from the surface of an old neutron star does not peak anymore in the X-ray band, the power of the Hubble Space Telescope allows one to observe it in the optical-UV range. Pavlov et al. (1996a) detected PSR B1929+20 at near-UV frequencies and showed that the observed flux corresponds to a temperature of about 0.2 MK, if the radiation is thermal. A candidate for the optical counterpart of PSR B0950+08 was also detected by the same authors, but its identification is less certain. Studying optical radiation from old nearby pulsars is very useful for understanding their thermal and non-thermal evolution.

No gamma-radiation has been detected even from the nearest old radio pulsars. Since the gamma-ray efficiency, $\epsilon_\gamma = L_\gamma/\dot{E}$, grows with age for young and middle-aged pulsars (for PSR 1055-52 it is almost 20%), it must have a break at about ~ 1 Myr not to exceed 100%. A reason for this break could be that the thermal surface photons are involved in the production of the observed gamma-rays, via Compton up-scattering of thermal photons by ultrarelativistic particles. As a neutron star cools down with growing age, the productions of gamma-rays, and hence the gamma-ray efficiency, decreases.

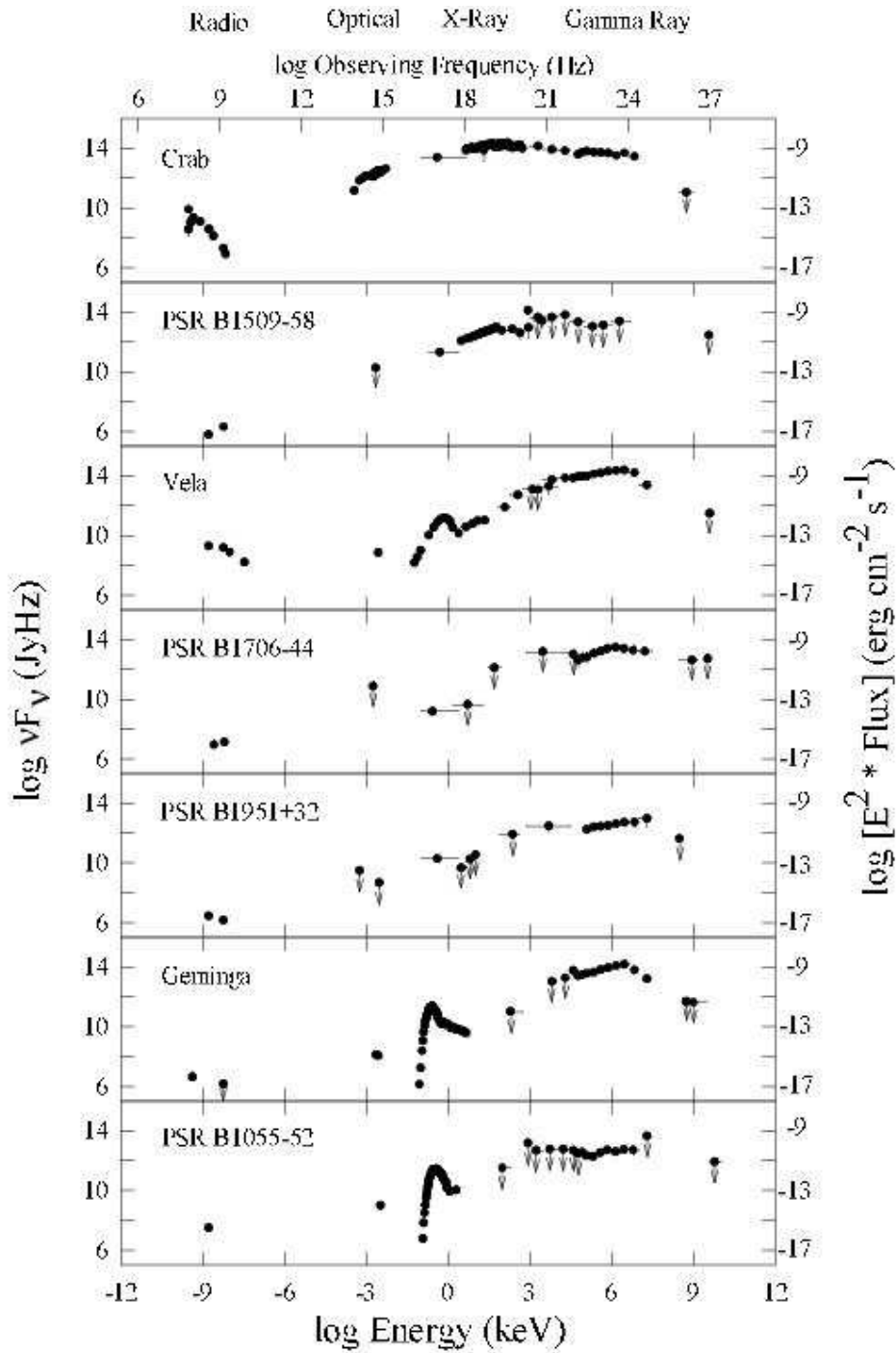


Figure 8.16: Multiwavelength spectra for the known gamma-ray pulsars, showing the observed power per logarithmic energy interval. All the spectra have in common that the high-energy radiation power rises from the optical to the X-ray band and that the maximum observed energy output is in the gamma-ray band, which demonstrates that emitting particles are accelerated to very high energies. (From Thompson et al. 1999).

8.3.4 Isolated Radio-quiet Neutron Stars

Analyzing the ROSAT PSPC observations of a field containing the molecular cloud R CrA ($d \approx 130$ pc), Walter, Volk & Neuhäuser (1996) noticed a bright point source, RX J1856–3754, projected

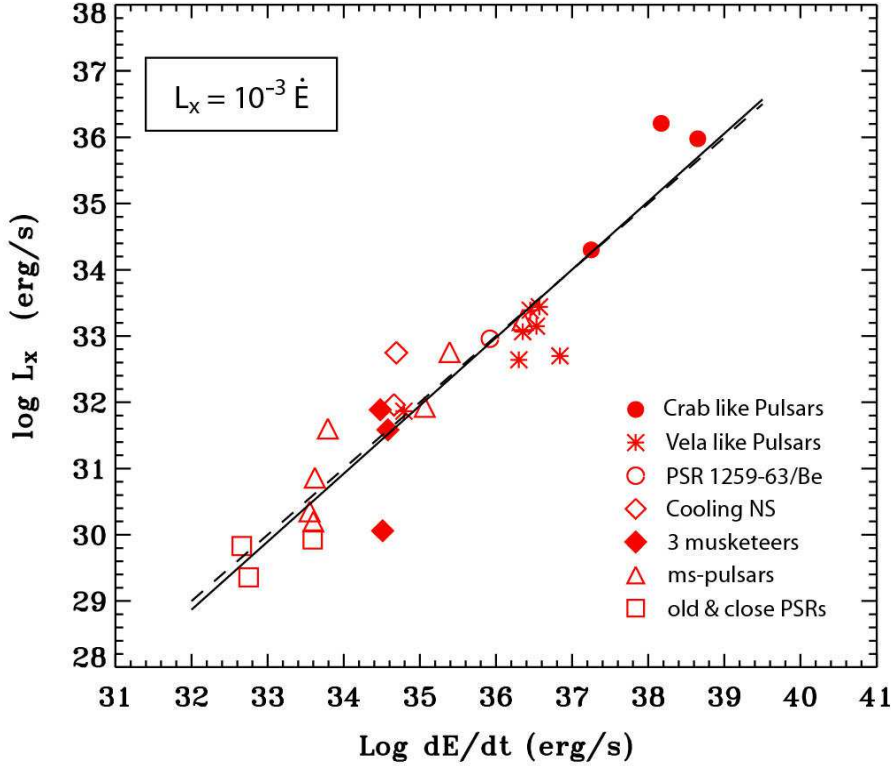


Figure 8.17: X-ray luminosity vs. spin-down energy loss for all rotation-powered pulsars detected by ROSAT. For the “three musketeers”, Geminga, PSR 0656+14 and 1055-52, the low energy thermal component has been subtracted from the data. The solid line represents $L_x(\dot{E}) \propto \dot{E}^{1.03}$, the dashed line $L_x(\dot{E}) = 10^{-3}\dot{E}$. Remarkably, all the detected pulsars, from the young Crab-like to the 10^9 year old millisecond pulsars follow the linear trend. (From Becker & Trümper 1997).

onto the cloud. Its spectrum is very soft – the best fit with a blackbody model gives a temperature of 0.66 MK and a luminosity of $\sim 5 \times 10^{31}$ erg s $^{-1}$ for a distance of 100 pc. Based on the lack of an optical counterpart brighter than $V \sim 23$, Walter et al. (1996) suggested that the source is a nearby isolated neutron star. As the objects described in 8.3.1.3, it is radio-quiet, but, contrary to those objects, it is not associated with any SNR (i.e., it is “truly isolated”). Since its temperature is much lower than the temperatures of the isolated neutron stars in supernova remnants, it is natural to assume that this object is much older, i.e. the neutron star has cooled down. Surprisingly, no pulsations of the X-ray radiation, expected from a neutron star with a “typical” magnetic field and favorable orientation of the magnetic and spin axes, were found. Pavlov et al. (1996b) fitted the X-ray spectrum with neutron star atmosphere models (see Section 8.2.2.3) and showed that different chemical compositions and different magnetic fields of the surface layers correspond to quite different optical magnitudes, $V=22 - 28$, and distances, 5 – 200 pc (for a neutron star radius of 10 km). Therefore, optical detection of this source (and other similar sources) would be a powerful tool to investigate the properties of neutron star atmospheres, while measuring the distance would allow one to evaluate the neutron star radius and constrain equation of state of the neutron star interiors.

A very faint, blue optical counterpart of RX J1856–3754 was discovered with the HST by Walter & Matthews (1997). The extremely large X-ray-to-optical flux ratio of $\sim 75,000$ proves unequivocally that this is indeed a neutron star. However, the optical magnitude, $V=25.7$, is considerably different from the predictions of the four atmosphere models considered by Pavlov et al. (1996b), which means that either the atmosphere has a different chemical composition and magnetic field or the temperature distribution is essentially non-uniform, e.g., because of

anisotropy of heat conduction in a very strong magnetic field. The nature of RX J1856–3754 became even more puzzling after its proper motion, 0.33 arcsec/yr, was measured (Walter et al. 2000). This proper motion corresponds to a transverse velocity of 140 km/s at $d = 100$ pc, too fast for accretion from ISM to be a major heating source. This means that RX J1856–3754 is a cooling neutron star, and with the apparent surface temperature of ≈ 0.7 MK it should be younger than 1 Myr, for the standard (slow) cooling models. On the other hand, projecting the proper motion backward, Walter et al. (2000) suggest that RX J1856–3754 and the well-known runaway O star ζ Oph originated from the same binary system disrupted by a supernova explosion about 2 Myr ago. A neutron star of such an age should have an apparent effective temperature < 0.4 MK, in contradiction with the current data.

The lack of pulsations, which could be explained by co-alignment of the magnetic and rotation axes, or the rotation axis and the line of sight, does not allow one to measure the spin period of RX J1856–3754. Fortunately, two other objects with similar properties, for which pulsations have been measured, were discovered with ROSAT – RX J0720–3125 with $P = 8.37$ s and RX J0420–5022 with $P = 22.7$ s (Haberl et al. 1996,1997,1999). Future measurements of their period derivatives will allow one to estimate their ages and elucidate the nature of these neutron stars. Particularly important will be deep optical/UV observations of these objects (a viable candidate for the optical counterpart of RX J0720–3125, with $B \approx 26.6$, has been found by Motch & Haberl 1998 and Kulkarni & van Kerkwijk 1998).

Three more objects of apparently the same class are known at the time of writing this article (see Table 8.1 and references therein). We expect that the number of detected radio-silent neutron stars will grow considerably in the near future, and we will be able to compare their properties with predictions of different models of neutron star evolution. One of the most important problems related to these objects is the source of energy which heats the radiating layers of the neutron stars up to 0.7 – 1.4 MK – it may be either the internal heat of relatively young cooling neutron stars, presumably with large magnetic fields, or accretion from the ISM onto old neutron stars (e.g., Treves et al. 2000). Presently, we cannot exclude the possibility that the observed six sources belong to two quite different classes, young coolers and old accretors.

8.3.5 Recycled Millisecond Pulsars

In the $P-\dot{P}$ parameter space, millisecond pulsars (ms-pulsars) are distinguished from the majority of ordinary-field pulsars by their short spin periods and small period derivatives, corresponding to very old spin-down ages of typically 10^9 – 10^{10} years and low magnetic field strengths of $\sim 10^8$ – 10^{10} G (cf. Fig. 8.2). More than $\sim 75\%$ of the known disk ms-pulsars are in binaries with a compact companion star, compared to $\approx 1\%$ binaries among the ordinary pulsars. This gives support to the idea that these neutron stars have been spun-up by angular momentum transfer during a past mass accretion phase (Bisnovatyi-Kogan & Komberg 1974; Alpar et al. 1982; Bhattacharya & van den Heuvel 1991). Indeed, the first accreting ms-pulsar, SAX J1808.4–3658, has been discovered with BeppoSAX (see van der Klis, this book). Presumably, these pulsars were originally among ordinary pulsars which would have turned off because of the loss of their rotational energy if they were not in close binaries; they are therefore often called the “recycled” pulsars.

By the end of 2000, about 100 recycled radio pulsars are known, of which 57 are located in the galactic plane (Camilo 1999; Edwards et al. 2000; Lommen et al. 2000; Lyne et al. 2000; Manchester et al. 2000). The others are in globular clusters (Kulkarni & Anderson 1996; Camilo et al. 2000) which provide a favorable environment for the recycling scenario (Rasio, Pfahl & Rappaport 2000). Only 10 of the 57 ms-pulsars in the galactic plane are solitary (including PSR B1257+12 which has a planetary system); the rest are in binaries, usually with a low-mass white dwarf companion. The formation of solitary recycled pulsars is not well-understood, but it is widely believed that either the pulsar’s companion was evaporated or the system was tidally disrupted after the formation of the ms-pulsar.

Recycled pulsars had been studied exclusively in the radio domain until the early 1990’s, when ROSAT, ASCA, EUVE, RXTE and BeppoSAX were launched. The first millisecond pulsar discovered as pulsating X-ray source was PSR J0437–4715 (Becker & Trümper, 1993), a nearby

5.75 ms pulsar which is in a binary with a low-mass white dwarf companion. Further detections followed, which, by the end of the century, sum up to almost 1/3 of all X-ray detected rotation-powered pulsars (cf. Table 8.2).

The available data suggest that the observed X-ray emission is likely to be generated by non-thermal processes in most of ms-pulsars. This is supported by observations of the 3.05 ms pulsar B1821–24 which is located in the globular cluster M28 (Kawai & Saito 1999), PSR B1937+21 – the fastest ms-pulsar known (Takahashi et al. 1999), and PSR J0218+4232 (Mineo et al. 2000). For these objects, power-law spectra and/or pulse profiles with narrow peaks have been measured (see Fig. 8.19). For PSR J0437–4715, the results of a recent Chandra observation suggest that the emission contains both the thermal component from the hot polar caps (Zavlin & Pavlov 1998) and a non-thermal component from the magnetosphere. The data on J2124–3358 do not allow to determine unambiguously which of the two components, thermal or nonthermal, is present in the observed emission. The 4.86 ms pulsar J0030+0451, which has spin parameters similar to those of J2124–3358, shows a high pulsed fraction of $69 \pm 18\%$. This, together with its Crab-like pulse profile and the gross similarity between its radio and X-ray profiles (cf. Fig. 8.19), suggests that the X-ray emission of this pulsar is dominated by the non-thermal component (Becker et al. 2000).

All other X-ray detected ms-pulsars (B1957+20, J1012+5307, B0751+18, J1744–1134 and J1024–0719) are identified only by their positional coincidence with the radio pulsar (Becker & Trümper 1999) and, in view of the low number of detected counts, do not provide much more than flux estimates. The power of XMM-Newton and Chandra is needed to explore their emission properties in more detail. However, the fact that all millisecond pulsars have roughly the same X-ray efficiency ($L_X/\dot{E} \sim 10^{-3}$) as ordinary pulsars (cf. Fig.8.17) supports the conclusion that, as a rule, the non-thermal X-ray radiation from their magnetospheres prevails over the thermal radiation from their polar caps (cf. Becker and Trümper 1997).

As far as the emission of gamma-rays from ms-pulsars is concerned, PSR J0218+4232 has been proposed to be the counterpart of the EGRET source 2EG J0220+4228 (Verbunt et al. 1996; Kuiper et al. 2000). The final verification, however, has to await the next gamma-ray missions, GLAST, and INTEGRAL, which are scheduled for the first decade of the new millennium. If J0218+4232 is indeed a gamma-ray pulsar, then, depending on the assumed emission model, 7 – 33% of its spin-down energy would go into the production of gamma-rays. No other ms-pulsars have been identified with gamma-ray sources so far, although according to the polar-cap and outer-gap emission models their predicted efficiencies should be even higher than that estimated for J0218+4232.

An important aspect of pulsar studies is searching for pulsar-wind nebulae (PWNe). So far, bow-shock PWNe have been firmly detected in H_α emission around PSR 1957+20 (Fruchter et al. 1992) and PSR J0437–4715 (Bell, Bailes & Bessel 1993). The bow-shock stand-off distance found in J0437–4715 is about $7''$ (Bell et al. 1995). Observations with the ROSAT HRI yielded a 3σ upper limit of $0.2 \times 10^{-3}\dot{E}$ for the X-ray emission from the nebula (Becker & Trümper 1999). Another PWN candidate is an object RX J1824.5–2452E near PSR B1821–24 (see Fig. 8.18). However, as the pulsar is located in a globular cluster, it is quite likely that this extended X-ray source is a superposition of spatially unresolved globular cluster sources (cataclysmic variables or low-mass X-ray binaries) rather than a plerion powered by the pulsar. We expect the true nature of RX J1824.5–2452E will be established in a deep Chandra observation of the globular cluster M28.

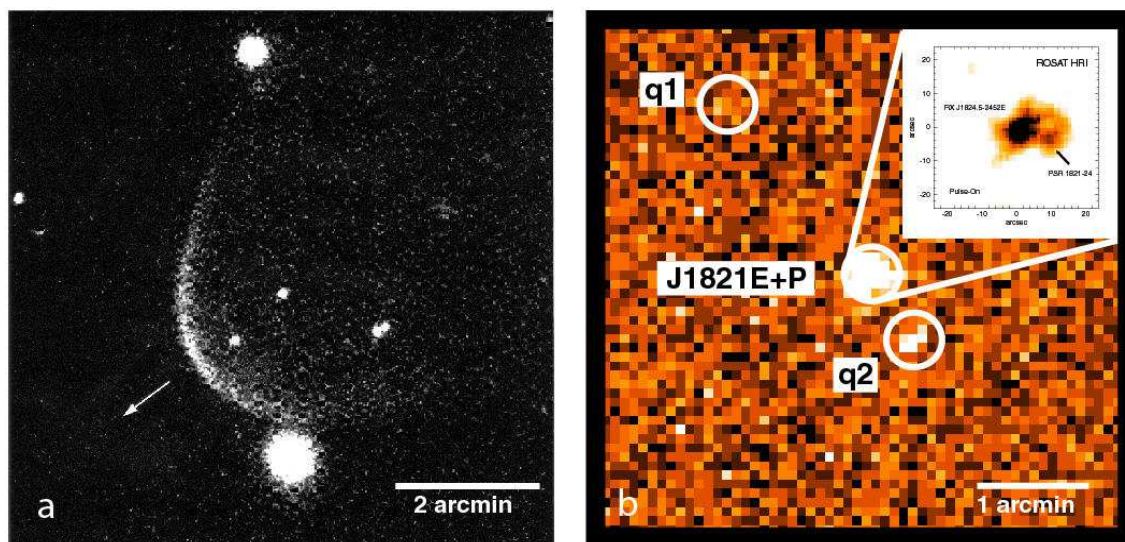


Figure 8.18: (a) Bow-shock nebula around PSR J0437–4715 as observed in the H_{α} emission (courtesy of A. Fruchter). The arrow indicates the direction of the pulsar’s proper motion. (b) $5' \times 5'$ ROSAT HRI image of the globular cluster M28. RX J1824.5–2452E, RX J1824.5–2452P, q1, and q2 indicate the positions of four X-ray sources, of which q1 and q2 are globular cluster background sources. The upper-right inset magnifies the core encompassing J1824E+P. Here, the ROSAT HRI data are oversampled at $1''$ bins and temporally phased to emphasize “pulse-on” events from the millisecond pulsar B1821-14 which is the faint source indicated by the arrow.

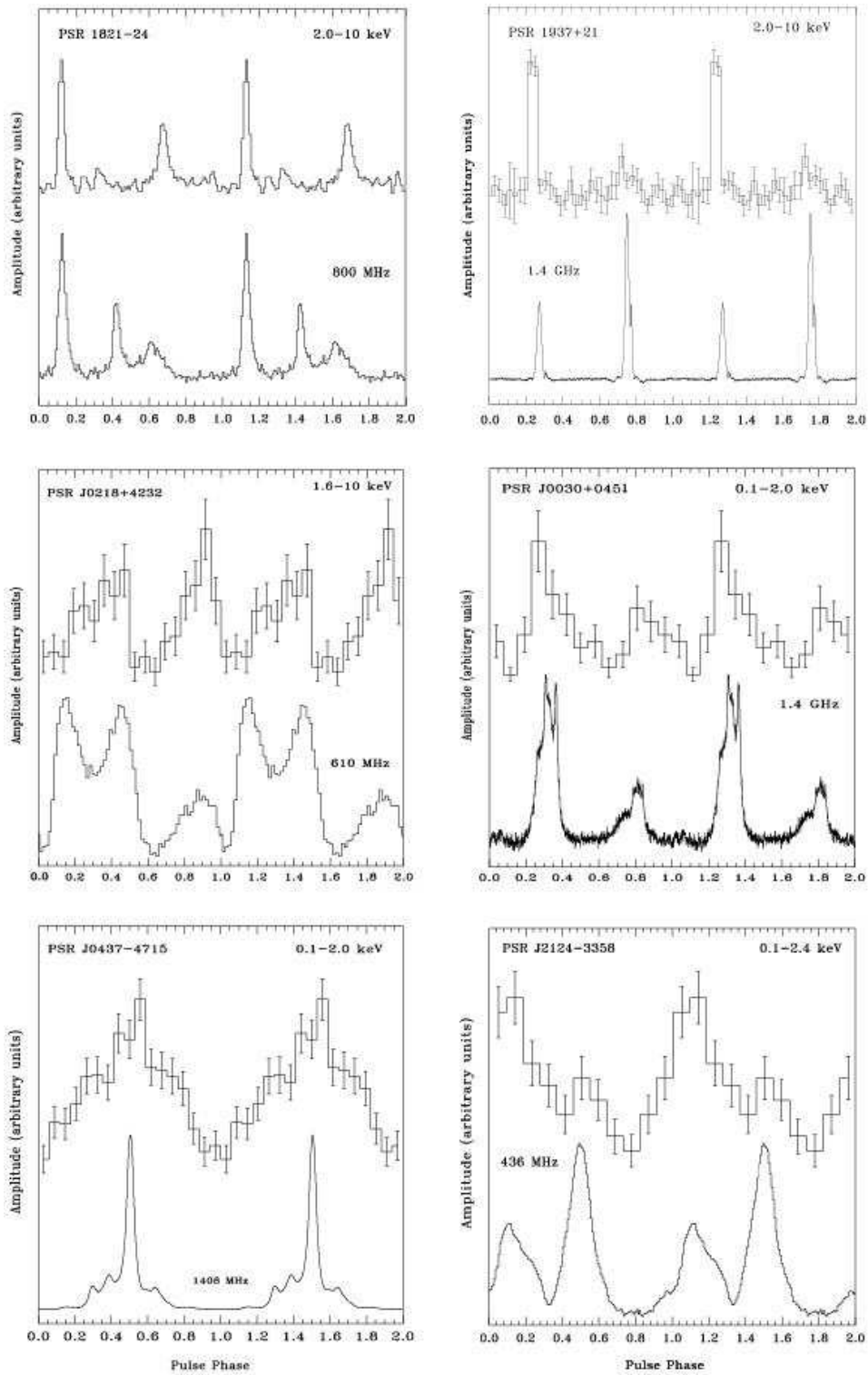


Figure 8.19: Integrated lightcurves for all ms-pulsars for which spin-modulated X-ray emission is detected. The upper phase histograms show the X-ray profiles in the given energy bands. The radio lightcurves are shown for comparison. Two phase cycles are shown for clarity. The relative phase between the radio and X-ray pulses is only known for PSR 1821-24 and PSR B1937+21 (Takahashi et al. 2001). In all other cases the phase alignment is arbitrary because of the lack of accurate satellite clock calibration.

8.4 Impressive Achievements and Great Expectations

Astronomers of our generation have been truly lucky — their collective efforts, generously supported by tax-payers of different countries, revolutionized our understanding of the Universe and its constituents, from clusters of galaxies to neutron stars. Fifty years ago, it was hard to imagine that neutron stars, very hypothetical objects at that time, not only would be discovered, but will also be studied in such a detail¹². The new vision of the Universe in general, and neutron stars in particular, has become possible only due to opening the new windows for observing the fascinating Cosmos — now we can study the Universe not only through the traditional, very narrow optical window, but also in radio, X-rays and gamma-rays. Without the X-ray and gamma-ray space observatories, our understanding of neutron stars, and many other objects virtually unknown half the century ago, would be much less complete. In particular, high-energy observations of the last decade of the 20-th century allowed us to understand that the world of neutron stars is not as simple as many astronomers had believed in the seventies and eighties (and some of them still believe). Neutron stars are not “just dim, heavy balls of ten kilometer radius”, as an expert in extragalactic astronomy claimed, explaining why proposals to observe neutron stars with the Hubble Space Telescope have been rejected so often. The neutron stars are not all alike — on the contrary, their properties and observational manifestations are no less diverse than those of usual stars and galaxies.

Amongst the more than 1,000 neutron stars discovered, about 100, including 60 isolated neutron stars (see Tables 8.1 and 8.2) have been observed at high energies with space observatories. These observations have firmly established that the properties of neutron stars are indeed highly unusual, particularly, their gravitational and magnetic fields are truly immense. We dare to predict that such exotic properties will never be achieved in terrestrial laboratories. Thus, neutron stars provide a unique opportunity to study the matter under extreme conditions. In particular, neutron stars can be viewed as cosmic laboratories for studying nuclear interactions, general relativity and superstrong magnetic and electric fields. This is the point where astrophysics and physics merge and cannot be separated from each other.

In spite of the impressive achievements of the neutron star physics/astrophysics, a lot of work still remains to be done in this recently emerged field. First, the evolution of neutron stars, starting from their violent birth in supernova explosions, is far from being well understood. Until very recently, a common prejudice had been that all neutron stars are born as active, rotation-powered pulsars, which slow down their rotation, eventually stop their activity and, after crossing a “death line”, get into the “pulsar graveyard”. A former pulsar remains in the graveyard forever, cool and quiet, unless it is captured by a flying-by star (e.g., in a globular cluster) and forms a close binary, where accretion onto the neutron star can spin it up (recycle) to so short periods that it again becomes an active pulsar.

The recent high-energy observations, however, show that the picture may not be so simple. In particular, it appears that many very young neutron stars are not active pulsars at all. The most recent example may be the central source of the 320-year-old Cassiopeia A supernova remnant (see Fig. 8.7; although at the time of writing of this article it is still not completely clear whether it is a neutron star or a black hole). Since such objects are not seen in radio, and are extremely faint in optical, they could not be observed until the onset of the X-ray astronomy era, which means that our perception of neutron star early evolution was very strongly biased in favor of much easier observable rotation-powered pulsars. Why are many (perhaps, the majority of) nascent neutron stars not active pulsars? Is it because they are indeed magnetars, whose superstrong magnetic field inhibits the pulsar activity? Or, on the contrary, their magnetic fields are so weak and/or rotation is so slow that the pulsar does not turn on? Or the pulsar activity is quenched by accretion of debris of the supernova explosion? Are the (apparently young) anomalous X-ray pulsars and soft

¹²Sachiko Tsuruta, who devoted her scientific life to studying the thermal evolution of neutron stars, recalls an episode of the mid-sixties, when she had finished her PhD thesis on the thermal evolution of neutron stars, which by that time were not expected to be observable. Says Tsuruta: “... By 1965, Bahcall and Wolf published papers that a neutron star cannot be seen if there are pions in the neutron star core. Soon after that I met John Bahcall at some conference, and he urged me to bet for discovering neutron stars, while he would bet against it. To my regret, I replied that a good Japanese woman should not bet. Then in 1967 a pulsar was discovered!”

gamma-ray repeaters indeed the magnetars or their unusual observational properties are due to quite different reasons, like a residual disk? To answer these questions, further observations, with more sensitive instruments of higher angular and energy resolution are needed.

One more set of evolutionary problems is associated with the generation and evolution of neutron star magnetic fields. Although there are no doubts that the very strong fields exist in many (if not all) neutron stars, there is no clear understanding of how they are generated. Why they are so different in different kinds of neutron stars (e.g., regular and recycled pulsars), what is their geometry, and do they decay during the neutron star life time? It should be mentioned that the direct measurements of the magnetic field have been possible only for neutron stars in binaries. What is called the “magnetic field” in, e.g., radio pulsars, is only an order-of-magnitude model-dependent estimate. Direct measurements of magnetic fields in isolated neutron stars, e.g. with the aid of spectral lines formed in their photospheres or from X-ray polarimetry, is one of very important goals for future observations.

One of the most important goals in studying isolated neutron stars is elucidating their internal composition (neutrons, quark-gluon plasma, strange matter, meson condensate ?) and the properties of the superdense matter (equation of state, nucleon superfluidity). Different equations of state correspond to different mass-radius dependences. Hence, the most direct way to determine the equation of state (which, in turn, depends on the internal composition) is measuring the masses and radii of neutron stars. One can constrain the radius from the star’s bolometric flux and effective temperature, provided the thermal radiation is not strongly “contaminated” by magnetospheric radiation of relativistic particles. The effective temperature can be determined from fitting the spectrum of the thermal radiation to neutron star atmosphere models. This method requires a good knowledge of the distance to the neutron star, which can be estimated from the radio dispersion measure if the neutron star is an active radio pulsar, or, much more precisely, from measuring its parallax.

The M/R ratio can be directly measured from the gravitational redshifts of spectral lines in the X-ray range. Measuring the redshifts would require X-ray detectors with high energy resolution and reliable computations for the energies of various atoms and ions in strong magnetic fields. Since the atomic states are greatly distorted by typical magnetic fields of neutron stars (and, consequently, spectral lines are strongly shifted from their zero-field positions), an independent measurement of the magnetic field (e.g., from fitting the continuum radiation to neutron star atmosphere models) would be necessary. The M/R ratio can also be evaluated from the analysis of the X-ray pulse profiles. Since the temperature is not uniform over the neutron star surface (due to anisotropy of the heat transfer in the crust or, for active pulsars, due to the accretion of relativistic particles onto the pole regions), the observed X-ray flux should vary with the rotation period. Because of the gravitational bending of photon trajectories, the shape of the pulse profile substantially depends on M/R . The observations will require high detector sensitivity ($\sim 10^4 - 10^5$ counts are needed to obtain accurate pulse profiles in a few energy ranges) and good time resolution ($\sim 10^{-5}$ s for millisecond pulsars). Finally, the properties of the internal matter can be constrained from measuring the effective temperatures of neutron stars of different ages. The thermal evolution of neutron stars depends substantially on the internal composition, equation of state, and nucleon superfluidity.

Of course, no firm conclusions about the internal properties can be drawn without studying the physical conditions in the surface layers of neutron stars: magnetic fields, temperatures, densities and, in particular, the chemical composition. Elucidating the chemical composition is also important in order to understand how neutron stars interact with their environment, both in their very young age, when a fraction of the supernova ejecta can fall back on the star’s surface, and during their whole life which may include some accretion episodes. The investigation of the surface layers (atmospheres) will require the analysis of soft X-ray spectra in terms of atmosphere models (hence, high sensitivity and spectral resolution of the detectors are needed). Important information about neutron stars can be obtained from their transverse velocities (proper motion) and parallaxes. These quantities have been measured for a handful of radio pulsars. X-ray telescopes with sub-arcsecond angular resolution will allow us to measure astrometric characteristics of nearby radio-quiet neutron stars.

After the 32 years of radio pulsar investigations, we still lack a consistent theory of the pulsar activity. New X-ray and gamma-ray data are expected to close this gap. In particular, X-ray radiation of many pulsars is due to relativistic particles in their magnetospheres, and studying the spectra and the pulse profiles of this radiation will allow us to determine the energy spectrum and directional pattern of the relativistic particles and, consequently, conditions in the pulsar acceleration zones and their temporal evolution. Furthermore, the X-ray range is most convenient for investigating the hot polar caps of radio pulsars, inevitable companions of the pulsar activity.

We expect that many of the above-formulated goals will be achieved with the aid of the satellite X-ray observatories Chandra and XMM-Newton, launched in 1999. First few months of Chandra observations have brought several important discoveries: the central compact object in Cas A, the unusual six-hour period of the central source of RCW 103, the discovery of the small-scale structure in the compact nebulae around the Crab and Vela pulsars. Much more discoveries, from both Chandra and XMM-Newton, will have been done by the time when this article is published. Furthermore, a number of new high-energy missions, GLAST, INTEGRAL, Constellation-X, and XEUS are being planned and, hopefully, will be launched within the next 10 – 20 years. Particularly useful for studying isolated neutron stars will be the Constellation-X and XEUS missions. For instance, the Constellation-X mission is planned to consist of six X-ray telescopes to be launched to the libration point in 2007–2008. Each of these payloads will combine the excellent angular resolution of Chandra with the large collecting area of XMM-Newton, so that we may expect a new revolution in X-ray astronomy in the second decade of the third millennium. Thus, we are looking forward to new discoveries which will raise additional questions — as such is the nature of the scientific cognition.

8.5 References

- Alpar M.A., Cheng A.F., Ruderman M.A., Shaham J., 1982, *Nature*, 300, 728
- Arons, J., Scharlemann, E.T. 1979, *ApJ*, 231, 854
- Arons, J., Tavani, M., 1993, *ApJ*, 403, 249
- Aschenbach, B. 1999, *IAU Circ.* #7249
- Aschenbach B., Brinkmann W. 1975, *A&A*, 41, 147
- Baade, W., Zwicky, F., 1934, *Proc. Nat. Acad. Sci.*, 20, 254
- Bhattacharya D., van den Heuvel E.P.J., 1991, *Phys. Rep.*, 203, 1
- Becker, W., & Trümper, J. 1993, *Nat*, 365, 528
- Becker, W., Trümper, J., Ögelman, H.B., 1993, in *Isolated Pulsars*, (eds K.A. Van Riper, R. Epstein & C. Ho), 104-109, (Cambridge University Press)
- Becker, W., 1995, Thesis, MPE-Report 260
- Becker, W., Aschenbach, B., in: *The Lives of the Neutron Stars*, eds. A.Alpar, U.Kilizoglu & J.van Paradijs, Kluwer Academic Publishers, p47
- Becker, W., Brazier, K., Trümper, J., 1995, *A&A*, 298, 528
- Becker, W., Trümper, J., 1997, *A&A*, 326, 682
- Becker, W., Trümper, J. 1999, *A&A*, 341, 803
- Becker, W., Kawai, N., Brinkmann, W., Mignani, R., 1999, *A&A*, 352, 532
- Becker, W., Trümper, J., Lommen, A.N., Backer, D.C., 2000, *ApJ*, 545, 1015
- Bell, J. 1977, *Ann. NY Acad. Sci.*, 302, 685
- Bell, J.F., Bailes, M., Bessel, M.S. 1993, *Nature*, 364, 603
- Bell, J.F., Bailes, M., Manchester, R.N., Weisberg, J.M., Lyne, A. 1995, *ApJ*, 440, L81
- Bertsch, D.L., et al. 1992, *Nature*, 357, 306
- Beskin, V.S., Gurevich, A.V., Istomin, Ya.N., 1993, *Physics of the Pulsar Magnetosphere*, Cambridge University Press, ISBN 0-521-41746-5
- Bignami, G.F., Caraveo, P.A., 1996, *Ann. Rev. Astron. Astrophys.* , 34, 331-381
- Bignami, G.F., Caraveo, P.A., Mignani, R., Edelstein, J., Bowyer, S., 1996, *ApJ*, 456, L111
- Bisnovatyi-Kogan G.S., Komberg B.V., 1974, *Sov. Astron.*, 18, 217
- Boyd P.T., van Citters G.W., Dolan J.F., et al., 1995, *ApJ* 448, 365
- Bowyer, S., 1990, in *Observatories in Earth Orbit and Beyond*, eds. Y. Kondo, Kluwer Academic Publishers, p.153
- Bowyer, C.S., Byram, E.T., Chubb, T.A., Friedman, H., 1964, *Nature*, 201, 1307
- Bradt, H.V., Rappaport, S., Mayer, W., Nather, R.E., Warner, B., Macfarlane, M., Kristian, J., 1969, *Nature*, 222, 728
- Bradt, H.V., Swank, J.H., Rothschild, R.E. 1990, *Adv. Space Res.*, 10, 297
- Brazier, K.T.S., Becker, W. 1997, *MNRAS*, 284, 335
- Brazier, K.T.S., Johnston, S. 1999, *MNRAS*, 305, 671
- Brinkmann, W., Ögelman, H. 1987, *A&A*, 182, 71
- Bulik, T., Pavlov, G.G. 1996, *ApJ*, 469, 373
- Butler, R.C., Scarsi, L., 1990, in *Observatories in Earth Orbit and Beyond*, eds Y. Kondo, Kluwer Academic Publishers, p.141
- Camilo, F. 1999, In *Pulsar Timing, General Relativity and the Internal Structure of Neutron Stars*, ed. Z. Arzoumanian, F. Van der Hooft, & E.P.J. van den Heuvel, [Amsterdam: Koninklijke Nederlandse Akademie van Wetenschappen], p. 115
- Camilo, F., Lorimer, D. R., Freire, P., Lyne, A. G., & Manchester, R. N., 2000, *ApJ*, 535, 975

- Caraveo, P.A., Bignami, G.F., Trümper, J. 1996, *A&A Rev.*, 7, 209
- Chakrabarty, D., Pivovarov, M.J., Hernquist, L.E., Heyl, J.S., Narayan, R. 2001, *ApJ*, in press
- Chandrasekhar, S., 1931, *ApJ*, 74, 81
- Cheng, A.F., Helfand, D.J. 1983, *ApJ*, 271, 271
- Cheng, K.S., Ho, C. & Ruderman, M.A., 1986a, *ApJ*, 300, 500
- Cheng, K.S., Ho, C. & Ruderman, M.A., 1986b, *ApJ*, 300, 522
- Chiu, H.Y., Salpeter, E.E., 1964, *Phys. Rev. Letters*, 12,413
- Clear, J., et al. 1987, *A&A*, 174, 85-99
- Cocke, W.J., Disney, M.J. Taylor, D.J. 1969 *Nature*, 221, 525
- Corbel, S., Wallyn, P., Dame, T.M., Durouchoux, P., Mahoney, W.A., Vilhu, O., Grindlay, J.E. 1997, *ApJ*, 478, 624
- Corbel, S., Chapus, C., Dame, T.M., Durouchoux, P. 1999, *ApJ*, 526, L29
- Corbet, R.H.D., Smale, A.P., Ozaki, M., Koyama, K., Iwasawa, K. 1995, *ApJ*, 443, 786
- Córdova F.A., Hjellming R.M., Mason K.O., Middleditch J., 1989, *ApJ*, 345, 451
- Danner, R., Kulkarni, S.R., Trümper, J. 1998, *AAS Meeting* 192, #43.09
- Daugherty, J.K., Harding, A.K. 1996, *ApJ*, 458, 278
- Edwards, R. T., 2000, in *Pulsar Astronomy - 2000 and Beyond*, ed. M.Kramer, N.Wex, and R.Wielebinski, [San Francisco : ASP], p.33
- Fenimore, E.E., Laros, J.G., Ulmer, A. 1994, *ApJ*, 432, 742
- Feroci, M., Frontera, F., Costa, E., Amati, L., Tavani, M., Rapisada, M., Orlandini, M. 1999, *ApJ*, 515, L9
- Fichtel, C.E., Hartman, R.C., Kniffen, D.A., Thompson, D.J., Bignami, G.F., Ogelman, H., Ozel, M.E., Tumer, T., 1975, *ApJ*, 198, 163
- Forman, W. et al., 1978, *ApJS*, 38, 357
- Fritz, G., Henry, R.C., Meekins, J.F., Chubb, T.A., Friedman, H., 1969, *Science*, 164, 709
- Fruchter, A.S., Bookbinder, J., Garcia, M.R., Bailyn, C.D., 1992, *Nature*, 359, 303
- Gaensler, B.M., Gotthelf, E.V., Vasisht, G. 1999, *ApJ*, 526, L37
- Garmire, G.P., Pavlov, G.G., Garmire, A.B., Zavlin V.E. 2000, *IAU Circ.* #7350
- Giacconi, R., Gursky, H., Paolini, F.R., Rossi B.B., 1962, *Phys. Rev. Lett.*, 9, 439
- Giacconi, R., Kellogg, E., Gorenstein, P., Gursky, H., Tananbaum, H., 1971, *ApJ*, 165, L27
- Giacconi, R., 1974, in *X-ray Astronomy*, eds R. Giacconi and H. Gursky, R. Reidel Publishing Company 1974, Holland, ISBN 90 277 02950
- Giacconi, R., et al, 1979, *ApJ*, 230, 540
- Glen, G., Sutherland, P. 1980, *ApJ*, 239, 671
- Glendenning, N.K., 1996, *Compact Stars*, Springer, ISBN-0-387-94783-3
- Gnedin, Yu.N., Pavlov, G.G. 1974, *Sov. Phys.-JETP*, 38, 903
- Gold, T., 1968, *Nature*, 218, 731
- Gold, T., 1969, *Nature*, 221, 25
- Gotthelf, E.V., Petre, R., Hwang, U. 1997, *ApJ*, 487, L175
- Gotthelf, E.V., Petre, R., Vasisht, G. 1999a, *ApJ*. 514, L107
- Gotthelf, E.V., Vasisht, G. 1998, *New Astronomy*, 3, 293
- Gotthelf, E.V., Vasisht, G., Dotani, T. 1999b, *ApJ*, 522, L49
- Gotthelf, E.V., Wang, Q.D. 2000, *ApJ*, 532, L117
- Gouiffes, C., Finley, J.P., Ögelman, H., 1992, *ApJ*, 394, 581

- Green D.A., 1998, ‘A Catalogue of Galactic Supernova Remnants (1998 September version)’, Mullard Radio Astronomy Observatory, Cambridge, United Kingdom
- Greenstein G., Hartke, G.J., 1983, ApJ, 271, 283
- Greiveldinger, C., Camerini, U., Fry, W., et al. 1996, ApJ, 465, L35
- Gregory, P.C., Fahlman, G.G. 1980, Nature, 287, 805
- Gudmundsson, E.H., Pethick, C.J., Epstein, R.I. 1983, ApJ, 272, 286
- Haberl, F., Motch, C., Buckley, D.A.H., Zickgraf, F.-J., Pietsch, W. 1997, A&A, 326, 662
- Haberl, F., Motch, C., Pietsch, W. 1998, Astron. Nachr., 319, 97
- Haberl, F., Pietsch, W., Motch, C. 1999, A&A, 351, L53
- Hailey, C.J., Craig, W.W. 1995, ApJ, 455, L151
- Halpern, J.P., Holt, S.S., 1992, Nature, 357, 222
- Halpern, J.P., Wang, F.Y.-H., 1997, ApJ, 477, 905
- Hambarian, V., Hasinger, G., Schope, A.D., Schulz, N.S., 2001, A&A, in press
- Harding, A.K., Muslimov, A.G. 1998, ApJ, 500, 862
- Harnden, F.R., Seward, F.D. 1984, ApJ, 283, 274
- Helfand, D.J., Becker, R.H. 1984, Nature, 307, 215
- Hill, R.J., et al. 1997, ApJ, 486, L99
- Hillier, R.R., Jackson, W.R., Murray, A., Redfern, R.M., Sale, R.G., 1970, ApJ, 162, L177
- Hoyle, R.A., Narlikar, J., Wheeler, J.A., 1964, Nature, 203, 914
- Hulleman, M.H., van Kerkwijk, M.H., Verbunt, F.V.M., Kulkarni, S. 2000, A&A, 358, 605
- Hurley, K., Kouveliotou, C., Cline, T., Mazets, E., Golenetskii, S., Frederiks, D.D., van Paradijs, J. 1999a, ApJ, 523, L37
- Hurley, K., Kouveliotou, C., Murakami, T., et al. 1999b, ApJ, 510, L111
- Hurley, K., Strohmayer, T., Kouveliotou, C., et al. 2000, ApJ, 528, L21
- Inan, U.S., Lehtinen, N.G., Lev-Tov, S.J., Johnson, M.P., Bell, T.F., Hurley, K. 1999, Geophys. Res. Lett., 26, 3357
- Iglesias, C.A., Rogers, F.J. 1996, ApJ, 464, 943
- Israel, G.L., Mereghetti, S., Stella, L. 1994, ApJ, 433, L25
- Israel, G.L., Covino, S., Stella, L., Campana, S., Haberl, F., Merghetti, S. 1999a, ApJ, 518, L107
- Israel, G.L., Oosterbroek, T., Angelini, L., Campana, S., Mereghetti, S., Parmar, A.N., Segreto, A., Stella, L., van Paradijs, J., White, N. 1999b, A&A, 346, 929
- Kanbach, G., et al. 1980, A&A, 90, 163
- Kanbach, G., et al. 1994, A&A, 289, 855
- Kaspi, V.M. 2000, in Pulsar Astronomy – 2000 and Beyond, eds. M. Kramer, N. Wex and R. Wielebinski, ASP Conference Series, v.202, p.485
- Kaspi, V.M., Chakrabarty, D., Steinberger, J. 1999, ApJ, 525, L33
- Kaspi V.M. Johnston S., Bell J., et al., 1994 ApJ423, L43
- Kawai, N., Tamura, K., 1996, in *IAU Colloquium 160*, eds S.Johnston, M.A.Walker and M.Bailes, p367
- Kawai, N., Saito, Y., 1999, Astro. Lett. and Communications, 38, 1
- Kellett, B.J., Branduardi-Raymont, G., Culhane, J.L., Mason, I.M., Mason, K.O., Whitehouse, D.R. 1987, MNRAS, 225, 199
- Kendziorra, E., Staubert, R., Pietsch, W., Reppin, C., Sacco, B., Trümper, J., 1977, ApJ, 217, L93
- Kniffen, D.A., 1990, in *Observatories in Earth Orbit and Beyond*, eds Y. Kondo, Kluwer Academic Publishers, p.63

- Kniffen, D.A., Hartman, R.C., Thompson, D.J., Bignami, G.F., Fichtel, C.E., Tümer T., Ögelman, H., 1974, *Nature*, 251, 397
- Koptsevich, A.B., Pavlov, G.G., Shibanov, Yu.A., Sokolov, V.V., Zharikov, S.V., Kurt, V.G. 2000, *A&A*, accepted
- Kouveliotou, C., Dieters, S., Strohmayer, T., van Paradijs, J., Fishman G.L., Meegan, C.A., Hurley, K., Kommers, J., Smith, I., Frail, D., Murakami, T. 1998, *Nature*, 393, 235
- Kriss, G.A., Becker, R.H., Helfand, D.J., Canizares, C.R. 1985, *ApJ*, 288, 703
- Kuiper, L., Hermsen, W., Krijger, J.M., Bennett, K., et al., 1999, *A&A*, 351, 119
- Kuiper L., Hermsen W., Verbunt F., Thompson, D.J., Stairs, I.S., Lyne, A.G., Strickman, M.S., Cusumano, G. 2000, *A&A*, 359, 615
- Kulkarni, S. R., Anderson, S. B. 1996, in *Dynamical Evolution of Star Clusters – Confrontation of Theory and Observations: IAU Symposium 174*, Kluwer Academic Publisher, p.181
- Kulkarni, S.R., Frail, D.A. 1993, *Nature*, 356, 33
- Kulkarni, S.R., van Kerkwijk, M.H. 1998, *ApJ*, 507, L49
- Kundt, W., Schaaf, R., 1993, *Ap & SpSc*, 200, 251
- Landau, L., 1932, *Phys.Z. Sowjetunion*, 1, 285
- Large, M.I., Voughan, A.E., Mills, B.Y., 1968, *Nature*, 220, 340
- Lattimer, J.M., Pethick, C.J., Prakash, M., Haensel, P. 1991, *Phys. Lett.*, 66, 2701
- Lommen, A.N., Zepka, A., Backer, D.C., Cordes, J.M., Arzoumanian, Z., McLaughlin, M., & Xilouris, K. 2000, *ApJ*, submitted
- Long K.S., Helfand D.J., 1979, *ApJ*, 234, L77
- Lyne A. G, Pritchard R. S, Smith F. G., 1988, *MNRAS*, 233, 667
- Lyne A. G, Pritchard R. S, Graham-Smith F., Camilo F., 1996, *Nature*, 381, 497
- Lyne, A. G., Camilo, F., Manchester, R. N., Bell, J. F., Kaspi, V. M., D'Amico, N., McKay, N. P. F., Crawford, F., Morris, D. J., Sheppard, D. C., & Stairs, I. H., 2000, *MNRAS*, 312, 698
- Manchester, R.N., et al. 1978, *MNRAS*, 184, 159
- Manchester, R. N., Lyne, A. G., Camilo, F., Kaspi, V. M., Stairs, I. H., Crawford, F., Morris, D. J., Bell, J. F., & D'Amico, N., 2000, in *Pulsar Astronomy - 2000 and Beyond*, ed. M.Kramer, N.Wex, and R.Wielebinski, [San Francisco : ASP], p.49
- Marsden, D., Rotschild, R.E., Lingenfelter, R.E. 1999, *ApJ*, 520, L107
- Marshall, F.E., Gotthelf, E.V, Zhang, W., Middleditch, J., Wang, Q.D., 1998, *ApJ*, 499, L179
- Martin, C., Halpern, J.P., Schiminovich, D. 1998, *ApJ*, 494, L211
- Mazets, E.P., et al. 1979a, *Nature*, 282, 587
- Mazets, E.P., Golenetskii, S.V., Guryan, Yu. 1979b, *Sov. Astron. Lett.*, 5(6), 343
- Mereghetti, S. 2000, In *The Neutron Star – Black Hole Connection*, NATO ASI Series, to be published (astro-ph/9911252)
- Mereghetti, S., Stella, L. 1995, *ApJ*, 442, L17
- Mereghetti, S., Bignami, G.F., Caraveo, P.A. 1996, *ApJ*, 464, 842
- Michel, F.C., 1991, *Theory of Neutron Star Magnetospheres*, University of Chicago Press, ISBN 0-226-52331-4
- Mignani, R., Caraveo, P.A., Bignami, G.F. 1997, *ApJ*, 474, L51
- Mineo, T., Cusumano, G., Kuiper, L., Hermsen, W., Massaro E., Becker, W., Nicastro, L., Sacco, B., Verbunt, F., Lyne, A.G., Stairs, I.H., Shibata, S. 2000, *A&A*, 355, 1053
- Mineo, T., Cusumano, G., Massaro, E., Nicastro, L., Parmar, A.N., Sacco, B., 1999, *A&A*, 348, 519
- Morrison, P., 1958, *Nuovo Cimento*, 7, 858

- Morrison, P., Olbert, S., Rossi, B., 1954, Phys.Rev., 94,440
- Motch, C., Haberl, F. 1998, A&A, 333, L59
- Motch, C., Haberl, F., Zickgraf, F.-J., Hasinger, G., Schwöpe, A.D. 1999, A&A, 351, 177
- Murakami, T., Kubo, S., Shibasaki, N., Takeshima, T., Yoshida, A., Kawai, N. 1999, ApJ, 510, L119
- Murray, S.S., Slane, P.O., Seward, D., Ransom, S.C., Gaensler, B.M., 2001, to appear in ApJ
- Neuhäuser, R., Trümper, J. 1999, A&A, 343, 151
- Ögelman, H., Finley, J.P., Zimmerman, H.U. 1993, Nature, 361, 136
- Ögelman, H., 1995, in *The Lives of Neutron Stars* eds A. Alpar, U. Kızıloğlu & J. van Paradijs, Kluwer Academic Publishers, p.101
- Oosterbroek, T., Parmar, A.N., Mereghetti, S., Israel, G.L. 1998, A&A, 334, 925
- Oppenheimer, J.R., Volkoff, G.M., 1939, Phys. Rev., 55, 374
- Ostriker, J.P., & Gunn, J.E. 1969, ApJ, 157, 1395
- Pacini, F., 1967, Nature, 216, 567
- Pacini, F., 1968, Nature, 219, 145
- Page, D., Applegate, J.L. 1992, ApJ, 394, L17
- Page, D., Shibanov, Yu.A., Zavlin, V.E. 1996, in *Röntgenstrahlung from the Universe*, MPE Report 263, p.173.
- Pavlov, G.G., Mészáros, P. 1993, ApJ, 416, 752
- Pavlov, G.G., Potekhin, Y.A. 1995, ApJ, 450, 883
- Pavlov, G.G., Shibanov, Yu.A. 1978, Sov. Astron., 22, 214
- Pavlov, G.G., Zavlin, V.E. 1997, ApJ, 490, L91
- Pavlov, G.G., Zavlin, V.E. 1999, IAU Circ. #7270
- Pavlov, G.G., Zavlin, V.E. 2000, ApJ, 529, 1011
- Pavlov, G.G., Zavlin, V.E. 2001, ApJ, to be published
- Pavlov, G.G., Shibanov, Yu.A., Ventura, J., Zavlin, V.E. 1994, A&A, 289, 847
- Pavlov, G.G., Shibanov, Y.A., Zavlin, V.E., Meyer, R.D., 1995, in *The Lives of Neutron Stars* eds A. Alpar, U. Kızıloğlu & J. van Paradijs, Kluwer Academic Publishers, p.71
- Pavlov, G.G., Stringfellow, G.S., Córdova, F.A. 1996a, ApJ, 467, 370
- Pavlov, G.G., Zavlin, V.E., Trümper, J., Neuhäuser, R. 1996b, ApJ, 472, L33
- Pavlov, G.G., Welty, A.D., Córdova, F.A. 1997, ApJ, 489, L75
- Pavlov, G.G., Sanwal, D., Garmire, G.P., Zavlin, V.E., Burwitz, V., Dodson, R. 2000a, AAS Meeting 196, #37.04
- Pavlov, G.G., Zavlin, V.E., Aschenbach, B., Trümper, J., Sanwal, D. 2000b, ApJ, 531, L53
- Petre, R., Kriss, G.A., Winkler, P.F., Canizares, C.R. 1982, ApJ, 258, 22
- Petre, R., Becker, C.M., Winkler, P.F. 1996, ApJ, 465, L43
- Plucinsky P.P., Snowden S.L., Aschenbach B., et al. 1996, ApJ, 463, 224
- Rajagopal, M., Romani, R.W. 1996, ApJ, 461, 327
- Rajagopal, M., Romani, R.W., Miller, M.C. 1997, ApJ, 479, 347
- Ramanamurthy, P.V., Fichtel, C.E., Harding, A.K., et al. 1996, A&AS, 120, 115
- Rasio, F.A., Pfahl, E.D., & Rappaport, S. 2000, ApJ, 532, L47
- Romani, R.W. 1987, ApJ, 313, 718
- Romani, R.W. 1996, ApJ, 470, 469
- Romani, R.W., Yadigaroglu, I.-A. 1995, ApJ, 483, 314

- Rosenfeld, L., 1974, in the Proceedings 16th Solvay Conference on Physics, eds F. Pacini, Editions de l'Universite de Bruxelles, p174
- Rothschild, R.E., Kulkarni, S.R., Lingenfelter, R.E. 1994, Nature, 368, 432
- Ruderman, M., Sutherland, P.G., 1975, ApJ, 196, 51
- Schwope, A.D., Hasinger, G., Schwarz, R., Haberl, F., Schmidt, M. 1999, A&A, 341, L51
- Seward, F.D. 1990, ApJSS, 73, 781
- Seward, F.D., Harnden, F.R. 1982, ApJ, 256, L45
- Seward, F.D., Harnden, F.R. 1994, ApJ, 421, 581
- Seward, F.D., Wang, Z.-R. 1988, ApJ, 332, 199
- Seward, F.D., Charles, P.A., Smale, A.P. 1986, ApJ, 305, 814
- Seward, F.D., Harnden, F.R., Helfand, D.J. 1984, ApJ, 287, L19
- Shearer, A., Redfern, R.M., Gorman, G., et al. 1997, ApJ, 487, L181
- Shibanov, Yu.A., Yakovlev, D.G. 1996, A&A, 309, 171
- Shibanov, Yu.A., Zavlin, V.E., Pavlov, G.G., Ventura, J. 1992, A&A, 266, 313
- Shibanov, Yu.A., Pavlov, G.G., Zavlin, V.E., Qin, L., Tsuruta, S. 1995, in Proc. 17-th Texas Symposium on Relativistic Astrophysics, ed. H. Bohringer, G. Morfill, & J. Trümper, Ann. NY Acad. Sci., 759, 291
- Sonobe, T., Murakami, T., Kulkarni, S.R., Aoki, T., Yoshida, A. 1994, ApJ, 436, L23
- Staelin, D.H., Reifenstein, III, E.C., 1968, Science, 162, 1481
- Strickman, M.S., Harding, A.K., de Jager, O.C. 1999, ApJ, 524, 373
- Sturmer, S.J., Dermer, C.D. 1994, ApJ, 420, L79
- Sturmer, S.J., Dermer, C.D., Michel, F.C. 1995, ApJ, 445, 736
- Sugizaki, M., Nagase, F., Torii, K., Kunigasa, K., Asanuma, T., Matsuzaki, K., Koyama, K., Yamauchi, S. 1997, PASJ, 49, L25
- Takahashi M., Shibata S., Torii K., Saito Y., Kawai N. 1998, IAU Circ. 7030
- Tanaka, Y., Inoue, H., Holt, S., 1994, PASJ, 46, L37
- Tananbaum, H. 1999, IAU Circ. #7246
- Tananbaum, H., Gursky, H., Kellogg, E.M., Levinson, R., Schreier, E., Giacconi, R. 1972, ApJ, 174, L143
- Taylor, B.G., Andersen, R.D., Peacock, A., Zobl, R. 1981, Space Sci. Rev., 30, 479
- Taylor, J.H., Manchester, R.N., Lyne, A.G., 1993, ApJSuppl., 89, 189
- Thompson, C., Duncan, R.C. 1995, MNRAS, 275, 255
- Thompson, C., Duncan, R.C. 1996, ApJ, 473, 322
- Thompson, D.J., Fichtel, C.E., Kniffen, D.A., Ögelman, H.B., 1975, ApJ, 200, L79
- Thompson, D.J., et al. 1999, ApJ, 516, 297
- Torii, K., Kunigasa, K., Katayama, K., Tsunemi, H., Yamauchi, S. 1998, ApJ, 503, 843
- Treves, A., Turolla, R., Zane, S., Colpi, M. 2000, PASP, 112, 297
- Trümper, J., Pietsch, W., Reppin, C., Voges, W., Staubert, R., Kendziorra, E. 1978, ApJ, 219, L105
- Trümper, J., 1983, Adv. Space Res., 2, 241
- Tsuruta S., 1998, Physics Reports, 292, 1
- Tucker, W. 1984, The Star Splitters, NASA SP-466
- Tuohy, I.R., Garmire, G.P. 1980, ApJ, 239, L107
- van Kerkwijk, M.H., Kulkarni, S.R., Matthews, K., Neugebauer, G. 1995, ApJ, 444, L33
- van Paradijs, J., Taam, R.W., van den Heuvel, E.P.J. 1995, A&A, 299, L41

- Vasisht, G., Gotthelf, E.V. 1997, ApJ, 486, L129
- Verbunt F., Kuiper L., Belloni T., et al. 1996, A&A, 311, L9
- Walter, F.M., Matthews, L.D. 1997, Nature, 389, 358
- Walter, F.M., Volk, S.J., Neuhäuser, R. 1996, Nature, 379, 233
- Walter, F.M., An, P., Lattimer, J., Prakash, M. 2000, in Highly Energetic Physical Processes and Mechanics for Emission from Astrophysical Plasmas, eds. P.C.H. Martens, S. Tsuruta and M.A. Weber, IAU Symp. 195, p.437
- Wang, Z.-R., Seward, F.D. 1984, ApJ, 285, 607
- Wang, Q.D., Gotthelf, E.V. 1998, ApJ, 509, L109
- Wang, F.Y.-H., Ruderman, M., Halpern, J.P., Zhu, T. 1998, ApJ, 498, 373
- Weber, F. 1999, Pulsars as Astrophysical Laboratories for Nuclear and Particle Physics, Institute of Physics, ISBN 0-7503-0332-8
- Weisskopf, M.C., Hester, J.J., Tennant, A.F., et al. 2000, ApJ, 536, L81
- White, N.E., Angelini, L., Ebisawa, K., Tanaka, Y., Ghosh, P. 1996, ApJ, 463, L83
- Wills, R.D., Bennett, K., Bignami, G.F., Bucccheri, R., Caraveo, P.A., Hermsen, W., Kanbach, G., Masnou, J.L., Mayer-Hasselwander, H.A., Paul, J.A., Sacco, B., 1982, Nature, 296, 723
- Woods, P.M., Kouveliotou, C., van Paradijs, J., Finger, M.H., Thompson, C. 1999a, ApJ, 518, L103
- Woods, P.M., Kouveliotou, C., van Paradijs, J., et al. 1999b, ApJ, 524, L55
- Woods, P.M., Kouveliotou, C., van Paradijs, J., et al. 1999c, ApJ, 527, L47
- Woods, P.M., Kouveliotou, C., van Paradijs, J., et al. 1999d, ApJ, 519, L139
- Yakovlev, D.G., Levenfish, K.P., Shibano, Yu.A. 1999, Physics-Uspekhi, 169, 825
- Yancopoulos, S., Hamilton, T.T., Helfand, D.J., 1994, ApJ, 429, 832
- Zavlin V.E., Pavlov G.G., 1998, A&A, 329, 583
- Zavlin, V.E., Pavlov, G.G., Shibano, Yu.A., Ventura, J., 1995a, A&A, 297, 441
- Zavlin, V.E., Shibano, Yu.A., Pavlov, G.G. 1995b, Astron. Lett., 21, 168
- Zavlin, V.E., Pavlov, G.G., Shibano, Yu.A. 1996, A&A, 315, 141
- Zavlin, V.E., Pavlov, G.G., Trümper, J. 1998, A&A, 331, 821
- Zavlin, V.E., Trümper, J., Pavlov, G.G. 1999, ApJ, 525, 959
- Zavlin, V.E., Pavlov, G.G., Sanwal, D., Trümper, J. 2000, ApJ, 540, L25
- Zavlin, V.E., Pavlov, G.G., Halpern, J.P. 2001, ApJ, submitted
- Zhang, B., & Harding, A.K. 2000, ApJ, 532, 1150